Rosenthal, Y., Holbourn, A.E., Kulhanek, D.K., and the Expedition 363 Scientists
Proceedings of the International Ocean Discovery Program Volume 363
publications.iodp.org

Data report: Middle to Lower Miocene radiolarian biostratigraphy in the Western Pacific Warm Pool at IODP Expedition 363 Site U1490: preliminary results[1]

Kenji M. Matsuzaki,[2, 3] Shin-ichi Kamikuri,[4] and Takuya Sagawa[5]

[1] Matsuzaki, K.M., Kamikuri, S., and Sagawa, T., 2023. Data report: Middle to Lower Miocene radiolarian biostratigraphy in the Western Pacific Warm Pool at IODP Expedition 363 Site U1490: preliminary results. In Rosenthal, Y., Holbourn, A.E., Kulhanek, D.K., and the Expedition 363 Scientists, Western Pacific Warm Pool. Proceedings of the International Ocean Discovery Program, 363: College Station, TX (International Ocean Discovery Program). https://doi.org/10.14379/iodp.proc.363.206.2023
[2] Atmosphere and Ocean Research Institute, University of Tokyo, Japan. **kmatsuzaki@g.ecc.u-tokyo.ac.jp**
[3] Also at Department of Earth and Planetary Science, Graduate School of Science, University of Tokyo, Japan.
[4] Faculty of Education, Ibaraki University, Japan.
[5] Institute of Science and Engineering, Kanazawa University, Japan.

Contents

Keywords
International Ocean Discovery Program, IODP, *JOIDES Resolution*, Expedition 363, Western Pacific Warm Pool, Site U1490, Middle to Early Miocene radiolarian biostratigraphy, radiolarian assemblages

References (RIS)

MS 363-206
Received 8 September 2022
Accepted 16 November 2022
Published 12 May 2023

Abstract

Because the western equatorial Pacific Ocean is famous for its calcareous oozes, various biostratigraphic studies on planktonic foraminifers and calcareous nannofossils have been conducted in this region. As a result, western equatorial Pacific Ocean–based studies have established that the tropical Pacific region drives the atmospheric circulation by high seawater temperature, strongly influencing the global climate. Based on this finding, a number of sites were cored in this region during International Ocean Discovery Program (IODP) Expedition 363. Shipboard results unexpectedly revealed that radiolarians are abundant and well preserved in sediment from Eauripik Rise Site U1490 between 220 and 350 m core depth below seafloor, Method A (CSF-A), within an interval of calcareous ooze composed primarily of calcareous nannofossils and foraminifers. Paleomagnetic reversal event and calcareous nannofossil and planktonic foraminiferal bioevents suggested that the interval from 220 to 350 m CSF-A corresponded to the Middle to Early Miocene. This study investigated radiolarian assemblages and the biostratigraphy of core catcher samples obtained from Hole U1490A between 250 and 350 m CSF-A. Notably, the last occurrence (LO) of *Artophormis gracilis* (Riedel) was confirmed at ~338 m CSF-A, demonstrating that the base of the site is older than 22.6 Ma in age. Additionally, the first occurrence (16.9 Ma) and LO (13.9 Ma) of *Calocyclas costata* Riedel were identified at 246.7 and 227.8 m CSF-A, respectively, and the LO of *Didymocyrtis prismatica* (Haeckel), indicating an age of 17.7 Ma, was recorded at 258.5 m CSF-A. We also calculate preliminary sedimentation rates based on the Early Miocene radiolarian biostratigraphy and provide taxonomic notes on radiolarian species.

1. Introduction

International Ocean Discovery Program (IODP) Site U1490 is located at the northern part of the Eauripik Rise (a stable ridge separating the East and West Caroline Basins). The site is situated at 05°48.95′N, 142°39.27′E at a water depth of 2341 m (Figure **F1**). Three holes were drilled at the site (Holes U1490A–U1490C), with Hole U1490A drilled the deepest, recovering almost 380 m of sediments spanning from recent to upper Oligocene (**Rosenthal et al.**, 2018b). Notably, the sediments collected from Hole U1490A contain calcareous microfossils (mainly nannofossils and foraminifers), siliceous microfossils (radiolarians, diatoms, and sponge spicules), clay minerals, and volcanic ash (**Rosenthal et al.**, 2018b).

Based on variations in the relative abundance of the major components cited above and relying on a combination of visual core description, microscopic examination of smear slides, scanning electron microscopy, magnetic susceptibility, natural gamma radiation, and color reflectance (**Rosenthal et al.**, 2018a), the lithology of the sediment collected from Hole U1490A was divided into three subunits (IA–IC). Subunit IA is about 185 m thick and includes a sequence of Upper Miocene to recent foraminifer-rich nannofossil ooze with small amounts of clay and siliceous microfossils (Figure **F2**) (**Rosenthal et al.**, 2018b). Subunit IB is about 78 m thick (185–263 m core depth below seafloor, Method A [CSF-A]) (Figure **F2**). In this subunit, clay minerals are a significant component of the sediment, with increasing abundances downhole spanning the Middle to Lower Miocene (**Rosenthal et al.**, 2018b). It was also observed that although the primary lithology in Subunit IB is clay-rich foraminifer-nannofossil ooze, siliceous microfossils such as sponge spicules and radiolarians are also important components of Subunit IB sediment (**Rosenthal et al.**, 2018b). Subunit IC is about 124 m thick (263–387 m CSF-A) and spans the upper Oligocene to Lower Miocene. Although the uppermost 10 m of Subunit IC is composed of greenish radiolarian-rich nannofossil ooze, the remainder of the subunit is radiolarian-rich chalk (**Rosenthal et al.**, 2018b).

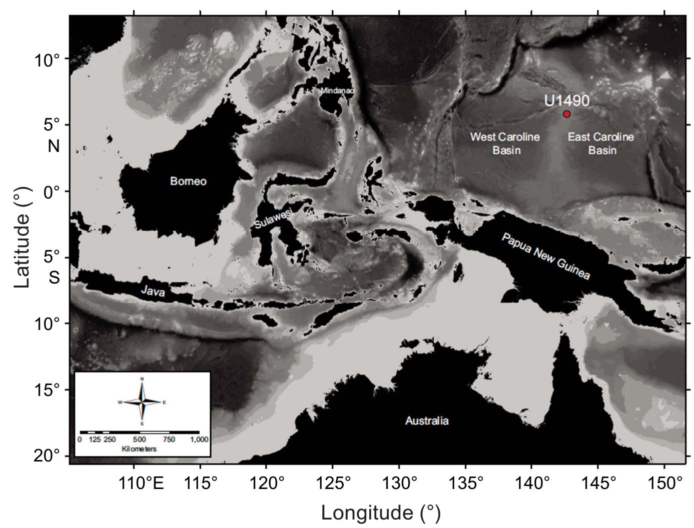

Figure F1. Location map and local bathymetry, Site U1490 (from Doyongan and Fernando, 2021).

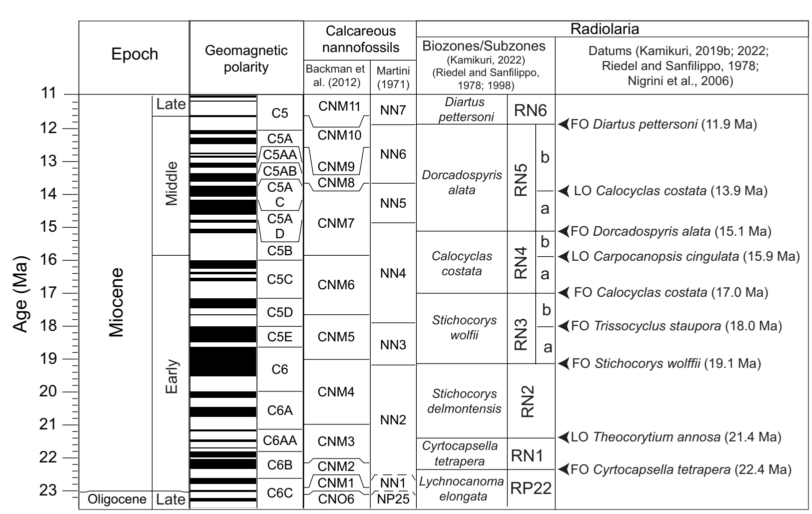

Figure F2. Tropical radiolarian biozones and key bioevents for Middle to Lower Miocene as defined by Riedel and Sanfilippo (1978), Nigrini et al. (2006), and Kamikuri (2019b, 2022) and calcareous nannofossil biozones of Backman et al. (2012) and Martini (1971). Geomagnetic polarity reversal events are also shown for calibration.

Calcareous nannofossil and planktonic foraminifer biostratigraphy, together with magnetostratigraphy, was conducted shipboard to date the collected sediment (**Rosenthal et al.**, 2018a). Investigations revealed that the sediment records a magnetic signal for all of Subunit IB, but little or no magnetic signal was found in Subunits IA and IC. Thus, the preliminary age model of Subunits IA and IC mainly relied on calcareous microfossil biostratigraphy. However, because the Middle Miocene sediment is surprisingly radiolarian rich, this provided an opportunity to examine radiolarian biostratigraphy at Site U1490. Therefore, this study aims to report preliminary radiolarian biostratigraphic results based on radiolarian assemblages from core catcher samples obtained from Subunits IA–IC. The newly established radiolarian biostratigraphy can help refine the age-depth model of Hole U1490A, particularly for Subunit IC, which has no magnetostratigraphic tie points and only a few calcareous microfossil biostratigraphic tie points. We also provide taxonomic notes for the abundant radiolarian species encountered during our preliminary analysis. Overall, this study is preliminary and will be followed up by analyzing higher resolution samples from Site U1490 to refine the radiolarian biostratigraphy.

2. Materials and methods

Samples from Site U1490 were prepared following the procedures described by Sanfilippo et al. (1985) and Kamikuri (2017, 2022). The dried and weighed sediment samples were placed in a beaker with 15% H_2O_2 to remove organic materials, after which a 3%–5% solution of hydrochloric acid was added to remove the calcareous fraction from the sediment. Subsequently, after the samples were washed and sieved through a 45 µm mesh, the dried sample was scattered randomly on a glass slide. Next, Norland optical adhesive 60 was used as a mounting medium for a 24–36 mm cover glass. Preservation of the radiolarian tests was assessed based on the following criteria (Table **T1**):

- Good (G): only minor fragmentation.
- Moderate (M): obvious fragmentation, but identification of species unimpaired.
- Poor (P): individual taxa exhibit considerable fragmentation, causing impossible identification of some species.

Relative abundances of individual taxa were classified based on the systematic examination of 500 radiolarians per sample (Kamikuri, 2022):

- Abundant (A): >10%.
- Common (C): >5%–10%.
- Few (F): 1%–5%.
- Rare (R): <1%.

3. Results

3.1. Radiolarian biozones

Based on the biostratigraphically useful radiolarian taxa occurrences in Hole U1490A (Plates **P1**, **P2**, **P3**, **P4**, **P5**; see **Appendix**; Table **T1**), we apply the tropical biostratigraphic scheme of Riedel and Sanfilippo (1970, 1978), Sanfilippo and Nigrini (1998), and Kamikuri (2022) to identify six radiolarian interval zones: the *Lychnocanoma elongata* Interval Zone (RP22), *Cyrtocapsella tetrapera* Interval Zone (RN1), *Stichocorys delmontensis* Interval Zone (RN2), *Stichocorys wolffii* Interval Zone (RN3), *Calocyclas costata* Interval Zone (RN4), and *Dorcadospyris alata* Interval Zone (RN5). Additionally, six interval subzones similar to those of Kamikuri (2022) were identified: the *Didymocyrtis prismatica* Interval Subzone (RN3a), *Trissocyclus stauroporus* Interval Subzone (RN3b), *Carpocanopsis cingulata* Interval Subzone (RN4a), *Dorcadospyris dentata* Interval Sub-

Table T1. Occurrence and preservation of biostratigraphically relevant radiolarian species in core catcher sediments, Hole U1490A. **Download table in CSV format.**

zone (RN4b), *Didymocyrtis mammifera* Interval Subzone (RN5a), and *Calocyclas caepa* Interval Subzone (RN5b).

3.1.1. Zone RP22: *Lychnocanoma elongata* Interval Zone (first identified by Riedel and Sanfilippo, 1970; amended by Riedel and Sanfilippo, 1978)

Definition: the top of this zone is defined by the first occurrence (FO) of *C. tetrapera* (Haeckel) (Figure **F2**). The base of this zone, although not identified at Site U1490 at least in core catcher material, is defined by the FO of *L. elongata* (Vinassa de Regny).

Interval: the base of Site U1490 at 382.8 m CSF-A is within this zone. The stratigraphic intervals assigned to this zone are between Samples 363-U1490A-43X-CC (380.06 m CSF-A) and 38X-CC (329.56 m CSF-A) (Table **T2**). During drilling of Core 43X, the extended core barrel (XCB) cutting shoe failed, resulting in the termination of drilling in Hole U1490A. Thus, the base of Site U1490 is within the *L. elongata* Interval Zone.

Important data: two other important bioevents were identified in this zone between Samples 363-U1490A-38X-CC and 39X-CC at a midpoint depth of 338.19 m CSF-A (Figure **F2**; Tables **T1**, **T2**): the last occurrence (LO) of *Artophormis gracilis* (Riedel) (22.6 Ma) and the FO of *Didymocyrtis bassanii* (Carnevale) (22.9 Ma).

Correlation and ages: the top of this zone is defined by the FO of *C. tetrapera*, which is typically located near the Chron C6C paleomagnetic reversal event (Figure **F2**). The upper *L. elongata* Interval Zone (RP22) corresponds to calcareous nannofossil Zones CNM1 (Backman et al., 2012) and NN1 (Martini, 1971) (Figure **F2**).

3.1.2. Zone RN1: *Cyrtocapsella tetrapera* Interval Zone (Riedel and Sanfilippo, 1978)

Definition: the base of this zone is defined by the FO of *C. tetrapera* (Figure **F2**), and the top of this zone is defined by the LO of *Theocorythium annosa* (Riedel).

Interval: stratigraphic intervals assigned to Zone RN1 are identified between Samples 363-U1490A-38X-CC (329.56 m CSF-A) and 35X-CC (308.71 m CSF-A) (Table **T2**).

Important data: three other important bioevents are identified in this zone. The FO of *Didymocyrtis tubaria* (Haeckel) (21.4 Ma) is situated between Samples 363-U1490A-35X-CC and 36X-CC at a midpoint depth of 312.52 m CSF-A (Figure **F2**; Tables **T1**, **T2**). The FO of *Calocyclas serrata* (Moore) (22.1 Ma) is identified between Samples 37X-CC and 38X-CC at a midpoint depth of 328.48 m CSF-A. Lastly, the FO of *Cyrtocapsella cornuta* (Haeckel), which is dated at 22.3 Ma, is found between Samples 36X-CC and 37X-CC at a midpoint depth of 321.87 m CSF-A.

Correlation and ages: this zone is defined by the FO of *C. tetrapera* and the LO of *T. annosa* and is typically correlated from the middle of Chron C6B to the Chron C6AA paleomagnetic reversal event (Figure **F2**). Investigations also revealed that the *C. tetrapera* Interval Zone (RN1) corresponds to the lower part of calcareous nannofossil Zone NN2 (Martini, 1971), as well as all of Zone CNM2 and the lower part of Zone CNM3 (Backman et al., 2012) (Figure **F2**).

3.1.3. Zone RN2: *Stichocorys delmontensis* Interval Zone (Riedel and Sanfilippo, 1978)

Definition: the base of this zone is defined by the LO of *T. annosa* (Riedel) (Figure **F2**), and the FO of *S. wolffii* Haeckel defines the top of this zone.

Interval: stratigraphic intervals assigned to this zone are identified between Samples 363-U1490A-35X-CC (308.90 m CSF-A) and 29F-CC (260.72 m CSF-A) (Table **T2**).

Important data: six other important bioevents were identified in this zone. First, the FO of *S. delmontensis* (Campbell and Clark) (20.7 Ma) and the LO of *C. serrata* (Moore) (20.5 Ma; Nigrini et al., 2006) are situated between Samples 363-U1490A-32X-CC and 33X-CC at a midpoint depth of 283.10 m CSF-A (Figure **F2**; Tables **T1**, **T2**). The FO of *Didymocyrtis violina* (Haeckel) (19.8

Table T2. Summary of recorded radiolarian bioevents, Hole U1490A. **Download table in CSV format.**

Ma), the LO of *Phormocyrtis alexandrae* O'Connor (19.0 Ma), and the LO of *C. tetrapera* (Haeckel) (18.9 Ma; Kamikuri, 2022) are identified between Samples 30F-CC and 31F-CC at a midpoint depth of 267.52 m CSF-A (Tables **T1**, **T2**). Additionally, the LO of *Dorcadospyris ateuchus* (Ehrenberg) (19.1 Ma) is recorded at 262.84 m CSF-A between Samples 29F-CC and 30F-CC.

Correlation and ages: the *S. delmontensis* Interval Zone (RN2) corresponds to the Chron C6AA and C6 paleomagnetic reversal event (Figure **F2**). This zone also corresponds to upper calcareous nannofossil Zone NN2 (Martini, 1971), as well as the upper part of Zone CNM3 and Zone CNM4 (Backman et al., 2012) (Figure **F2**).

3.1.4. Zone RN3: *Stichocorys wolffii* Interval Zone (Riedel and Sanfilippo, 1978)

Definition: the base of this zone is defined by the FO of *S. wolffii* Haeckel, and the top is defined by the FO of *Calocyclas costata* Riedel (Figure **F2**).

Interval: stratigraphic intervals are identified between Samples 363-U1490A-29F-CC (260.72 m CSF-A) and 27H-CC (251.4 m CSF-A) (Table **T2**).

Important data: four other important bioevents are identified in this zone: the FO of *T. stauroporus* Haeckel (18.0 Ma), which is situated between Samples 363-U1490A-28F-CC and 29F-CC at a midpoint depth of 258.36 m CSF-A (Figure **F2**; Tables **T1**, **T2**), the LOs of *D. prismatica* (Haeckel) (17.7 Ma) and *Thamnospyris schizopodia* (Haeckel) at 253.70 m CSF-A between Samples 27H-CC and 28F-CC (Figure **F2**; Tables **T1**, **T2**), and the LO of *Cyrtocapsella elongata* at 246.61 m CSF-A between Samples 26H-CC and 27H-CC.

Correlation and ages: the *S. wolffii* Interval Zone (RN3) corresponds to the Chron C6/C5C paleomagnetic reversal event (Figure **F2**). This zone also corresponds to upper calcareous nannofossil Zone NN3 and the lower part of Zone NN4 (Martini, 1971) and encompasses Zone CNM5 and the lower part of Zone CNM6 (Backman et al., 2012) (Figure **F2**).

Remarks: previous studies conducted in the Indian Ocean showed that it was possible to conduct precise correlations between data from radiolarians and calcareous nannofossils using Lower Miocene core sequences. Hence, based on precise new radiolarian data, Kamikuri (2022) divided the *S. wolffii* Interval Zone (RN3) into two subzones named the *D. prismatica* Interval Subzone (RN3a) and the *T. stauroporus* Interval Subzone (RN3b). Similarly, this study also identifies these subzones.

3.1.4.1. Subzone RN3a: *Didymocyrtis prismatica* Interval Subzone (Kamikuri, 2022)

Definition: the FO of *S. wolffii* Haeckel defines the base of this subzone, and the top is defined by the FO of *T. stauroporus* Haeckel (Figure **F2**).

Interval: stratigraphic intervals are identified between Samples 363-U1490A-29F-CC (260.72 m CSF-A) and 28F-CC (256.0 m CSF-A).

Correlation and ages: the *T. stauroporus* Interval Subzone (RN3a) corresponds to calcareous nannofossil Zones NN3 (Martini, 1971) and CNM5 (Backman et al., 2012) (Figure **F2**).

3.1.4.2. Subzone RN3b: *Trissocyclus stauroporus* Interval Subzone (Kamikuri, 2022)

Definition: the base of this subzone is defined by the FO of *T. stauroporus* Haeckel, and the top is defined by the FO of *Calocyclas costata* (Riedel) (Figure **F2**).

Interval: stratigraphic intervals are identified between Samples 363-U1490A-28F-CC (256.0 m CSF-A) and 26H-CC (241.8 m CSF-A) (Table **T2**).

Important data: the LO of *Cyrtocapsella elongata* (Nakaseko) at 246.61 m CSF-A between Samples 363-U1490A-26H-CC and 27H-CC is observed in this subzone.

Correlation and ages: the *D. prismatica* Interval Subzone (RN3b) corresponds to the lower part of calcareous nannofossil Zone NN4 (Martini, 1971) and the lower part of the Zone CNM6 (Backman et al., 2012) (Figure **F2**).

3.1.5. Zone RN4: *Calocyclas costata* Interval Zone (Riedel and Sanfilippo, 1970; amended by Riedel and Sanfilippo, 1978)

Definition: the base of this zone is defined by the FO of *Calocyclas costata* Riedel (Figure **F2**), and the top of this zone is defined by the evolutionary transition (ET) from *D. dentata* Haeckel to *D. alata* (Riedel) (Figure **F2**).

Interval: stratigraphic intervals are identified between Samples 363-U1490A-26H-CC (241.8 m CSF-A) and 25H-CC (232. 48 m CSF-A) (Table **T2**).

Important data: two other important bioevents are identified in this zone: the FO of *L. elongata* (Vinassa de Regny) and the LO of *C. cingulata* Riedel and Sanfilippo (18.9 Ma; Kamikuri, 2022) situated between Samples 363-U1490A-25H-CC and 26H-CC at a midpoint depth of 237.15 m CSF-A (Figure **F2**; Tables **T1**, **T2**).

Correlation and ages: the *Calocyclas costata* Interval Zone (RN4) corresponds to the Chron C5C/C5B paleomagnetic reversal event (Figure **F2**). This zone also corresponds to upper calcareous nannofossil Zone NN4 (Martini, 1971), as well as Zone CNM6 and the lower part of Zone CNM7 (Backman et al., 2012) (Figure **F2**).

Remarks: Kamikuri (2022) further divided the *Calocyclas costata* Interval Zone (RN4), relying on the LO of *C. cingulata* Riedel and Sanfilippo, into two subzones: the *C. cingulata* Interval Subzone (RN4a) and the *D. dentata* Interval Subzone (RN4b). Interestingly, this study identifies the LO of *C. cingulata* Riedel and Sanfilippo and the LO of *S. diaphanes* (Sanfilippo et al., 1985) between Samples 363-U1490A-25H-CC and 26H-CC at a midpoint depth of 237.3 m CSF-A (Tables **T1**, **T2**). This depth corresponds to the top of the *Calocycletta costata* Interval Zone (RN4) at Site U1490, indicating that the sedimentation rates at around 240 m CSF-A were low and that analysis of additional samples between the core catcher samples is required to define the subzones accurately. Magnetostratigraphy for this time interval also suggested low sedimentation rates between 200 and 250 m CSF-A (**Rosenthal et al.**, 2018b).

3.1.6. Zone RN5: *Dorcadospyris alata* Interval Zone (Riedel and Sanfilippo, 1970; amended by Riedel and Sanfilippo, 1978)

Definition: the base of this zone is defined by the ET from *D. dentata* Haeckel to *D. alata* (Riedel), and the top of this zone is defined by the FO of *Diartus petterssoni* (Riedel and Sanfilippo) (Figure **F2**).

Interval: the top of this zone could not be identified in Hole U1490A because of the poor preservation of radiolarians from samples shallower than Sample 363-U1490A-23H-CC. However, stratigraphic intervals assigned to this zone are still identified between Samples 25H-CC (232.48 m CSF-A) and 23H-CC (213.47 m CSF-A) (Table **T2**).

Remarks: previously, Kamikuri (2022) divided the *D. alata* Interval Zone (RN5) into two subzones, relying on the LO of *Calocyclas costata* (Riedel): the *D. mammifera* Interval Subzone (RN5a) and the *C. caepa* Interval Subzone (RN5b). Following this previous research, this study identifies the LO of *Calocyclas costata* Riedel between Samples 363-U1490A-24H-CC and 25H-CC at a midpoint depth of 227.73 m CSF-A (Tables **T1**, **T2**), with the *D. mammifera* Interval Subzone (RN5a) being the uppermost subzone.

3.1.6.1. Subzone RN5a: *Didymocyrtis mammifera* Interval Subzone (Kamikuri, 2022)

Definition: the base of this subzone is defined by the ET from *D. dentata* Haeckel to *D. alata* (Riedel), and the top is defined by the LO of *Calocyclas costata* (Riedel) (Figure **F2**).

Interval: stratigraphic intervals are identified between Samples 363-U1490A-25H-CC (232.48 m CSF-A) and 24H-CC (222.98 m CSF-A).

Important data: two other important bioevents are identified in this zone: the LOs of *D. tubaria* (Haeckel) and *D. violina* (Haeckel) situated between Samples 363-U1490A-24H-CC and 25H-CC at a midpoint depth of 227.73 m CSF-A (Figure **F2**; Tables **T1**, **T2**).

Correlation and ages: the *D. mammifera* interval Subzone (RN5a) corresponds to the Chron C5AD paleomagnetic reversal event (Figure **F2**). Investigations also revealed that the *D. mammifera* Interval Subzone (RN5a) corresponds to upper calcareous nannofossil Zone NN5 (Martini, 1971) and the upper part of Zone CNM7 (Backman et al., 2012) (Figure **F2**).

Remarks: the RN5a Interval Subzone lower boundary was defined by the ET from *D. dentata* to *D. alata* (Riedel and Sanfilippo, 1978). However, in this study, *D. dentata* was not observed in any of the 20 core catcher samples analyzed. Thus, we use the FO of *D. alata* instead. Nevertheless, analysis of additional samples from between core catchers will focus on the occurrence of *D. dentata*, despite *D. dentata* being rare or absent in some regions of the Indian Ocean (Kamikuri, 2022; S. Kamikuri, pers. comm., 2022).

3.1.6.2. Subzone RN5b: *Calocyclas caepa* Interval Subzone (Kamikuri, 2022)

Definition: the base of this subzone is defined by the LO of *Calocyclas costata* (Riedel) (Figure **F2**), and the top is defined by the FO of *D. petterssoni* (Riedel and Sanfilippo) (Figure **F2**).

Interval: Sample 363-U1490A-24H-CC (223.1 m CSF-A).

3.2. Updated Early Miocene age-depth model for Site U1490

A shipboard age-depth model was developed for Site U1490 using a combination of calcareous nannofossil and planktonic foraminifer biostratigraphy together with magnetostratigraphy. The magnetostratigraphy was particularly well defined between 197.0 (Subchron C5r.1r; ~11.056 Ma) and 263.30 m CSF-A (Chron C6n; 18.748 Ma), allowing for well-constrained sedimentation rates for the Miocene (Figure **F3**; **Rosenthal et al.**, 2018b). However, deeper than 263.3 m CSF-A (18.748 Ma), no more paleomagnetic reversal events were identified and only a few planktonic foraminifer and calcareous nannofossil bioevents were recorded, resulting in poorer age constraint for the interval between 263 and 350 m CSF-A. Recently, **Doyongan and Fernando** (2021) reported a revised nannofossil biostratigraphy for the Miocene and thus improved the accuracy of the age model.

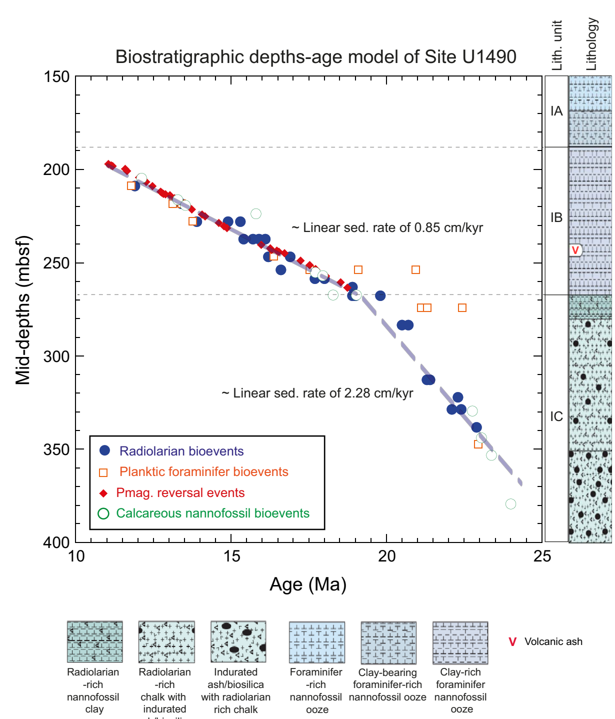

Figure F3. Age-depth model between ~200 and 350 m CSF-A based on paleomagnetic reversal events and planktonic foraminifer, calcareous nannofossil, and radiolarian bioevents, Site U1490.

Table T3. Tie points used to reconstruct Hole U1490A age-depth model. **Download table in CSV format.**

For further improvement of the age-depth model, we report 14 radiolarian bioevents between 263 and 350 m CSF-A for Hole U1490A that further constrain revised nannofossil biostratigraphy–based sedimentation rates for the Lower Miocene core sequences (Table **T3**).

There is generally good correspondence between radiolarian, calcareous nannofossil, and planktonic foraminifer bioevents for Hole U1490A (Figure **F3**), although there are some disparities with planktonic foraminifer ages between 250 and 265 m CSF-A (Figure **F3**). Such disparities correspond to changes in lithology, including a transition from clay-rich foraminifer-nannofossil ooze to radiolarian-rich nannofossil clay/radiolarian-rich chalk. However, because radiolarian ages fit well with paleomagnetic reversal events and calcareous nannofossil ages, we assume our preliminary results are reliable and allow us to compute preliminary sedimentation rates for depth intervals between 260 and 350 m CSF-A based on radiolarian bioevents. In lithologic Subunit IC, which is the oldest subunit (approximately between 350 and 270 m CSF-A), sedimentation rates were approximately 2.28 cm/ky (Figure **F3**). Sedimentation rates decreased at 270.3 m CSF-A to around 0.9 cm/ky, and this rate was maintained to 200 m CSF-A, which corresponds to lithologic Subunit IB (Figure **F3**). This decrease in sedimentation rate is close to the lithology transition from radiolarian-rich chalk with indurated ash/biosilica to radiolarian-rich nannofossil clay. These sedimentation rates could be improved in the future by additional refinement of the radiolarian biostratigraphy for the Lower Miocene using higher resolution samples.

4. Acknowledgments

This work uses samples and data provided by the International Ocean Discovery Program (IODP). This work was supported by Japan Society for the Promotion of Science (JSPS) Grant 19KK0089 awarded to Kenji M. Matsuzaki and in part by JSPS Grant 18H01279 awarded to Takuya Sagawa. We thank the IODP core curators at the Kochi Core Center (Japan) for providing samples as well as the IODP Expedition 363 science party. We also thank Drs. Ann Holbourn and Wolfgang Kuhnt for helpful advice. Lastly, we thank the editor, Dr. Denise Kulhanek, for reviewing and editing our manuscript and the reviewer, Dr. Johan Renaudie, for helpful and critical comments about radiolarian species taxonomy.

References

Backman, J., Raffi, I., Rio, D., Fornaciari, E., and Pälike, H., 2012. Biozonation and biochronology of Miocene through Pleistocene calcareous nannofossils from low and middle latitudes. Newsletters on Stratigraphy, 45(3):221–244. **https://doi.org/10.1127/0078-0421/2012/0022**

Bjørklund, K.R., and Goll, R.M., 1979. Internal skeletal structures of Collosphaera and Trisolenia: a case of repetitive evolution in the Collosphaeridae (Radiolaria). Journal of Paleontology, 53(6):1293–1326. **https://www.jstor.org/stable/1304135**

Boltovskoy, D., and Jankilevich, S.S., 1985. Radiolarian distribution in east equatorial Pacific plankton. Oceanologica Acta, 8(1):101–123.

Campbell, A.S., and Clark, B.L., 1944. Miocene radiolarian faunas from southern California. Special Paper - Geological Society of America, 51.

Carnevale, P., 1908. Radiolarie e silicoflagellati di Bergonzano (Regio Emilia). Memorie del Reale Instituto Veneto di Scienze, Lettere ed Arti, 28(3):1–46.

Caulet, J.P., 1979. Les dépôts à radiolaires d'âge Pliocène supérieur à Pleistocène dans l'océan Indien central: Nouvelle zonation biostratigraphique. Memoires du Museum National d'Histoire Naturelle Serie C Sciences de la Terre, 43:119–141.

Caulet, J.P., 1986. A refined radiolarian biostratigraphy for the Pleistocene of the temperate Indian Ocean. Marine Micropaleontology, 11(1–3):217–229. **https://doi.org/10.1016/0377-8398(86)90016-2**

Chen, P.-H., 1975. Antarctic radiolaria. In Hayes, D.E., Frakes, L.A., et al., Initial Reports of the Deep Sea Drilling Project. 28: Washington, DC (US Government Printing Office), 437–513. **https://doi.org/10.2973/dsdp.proc.28.111.1975**

Doyongan, Y.I.L., and Fernando, A.G.S., 2021. Data report: refinement of calcareous nannofossil biostratigraphy from the late Oligocene to the Pleistocene, IODP Expedition 363 Hole U1490A. In Rosenthal, Y., Holbourn, A.E., Kulhanek, D.K., and the Expedition 363 Scientists, Western Pacific Warm Pool. Proceedings of the International Ocean

Discovery Program, 363: College Station, TX (International Ocean Discovery Program). **https://doi.org/10.14379/iodp.proc.363.204.2021**

Dreyer, F., 1889. Die Pylombildungen in vergleichend-anatomischer und entwicklugs-geschichtlicher Beziehung bei Radiolarien und bei Protisten überhaupt, nebst System und Beschreibung neuer und der bis jetzt bekannten pylomatischen Spummellarien. Jenaische Zeitschrift für Naturwissenschaft herausgegeben von der medizinisch-naturwissenschaftlichen Gesellschaft zu Jena, 23:77–214.

Ehrenberg, C.G., 1846. Über eine halibiolithische, von Herrn R. Schomburgk entdeckte, vorherrschend aus mikroskopischen Polycystinen gebildete, Gebirgsmasse von Barbados. Bericht über die zur Bekanntmachung geeigneten Verhandlungen der Königlich Preußischen Akademie der Wissenschaften zu Berlin, 1847:382–385.

Ehrenberg, C.G., 1847. Über die mikroskopischen kieselschaligen Polycystinen als mächtige Gebirgsmasse von Barbados und über das Verhältniss der aus mehr als 300 neuen Arten bestehenden ganz eigenthümlichen Formengruppe jener Felsmasse zu den jetzt lebenden Thieren und zur Kreidebildung. Eine neue Anregung zur Erforschung des Erdlebens. Bericht über die zur Bekanntmachung geeigneten Verhandlungen der Königlich Preußischen Akademie der Wissenschaften zu Berlin, 1847:40–61.

Ehrenberg, C.G., 1861. Über die organischen und unorganischen Mischungsverhältnisse des Meeresgrundes in 19800 Fuss Tiefe nach Lieut. Brookes Messung. Monatsberichte der Königlich Preußischen Akademie der Wissenschaften zu Berlin, 1860:765–774.

Ehrenberg, C.G., 1874. Grössere Felsproben des Polycystinen-Mergels von Barbados mit weiteren Erläuterungen. Monatsberichte der Königlich Preußischen Akademie der Wissenschaften zu Berlin, 1873:213–262.

Ehrenberg, C.G., 1876. Fortsetzung der mikrogeologischen Studien als Gesammt-Übersicht der mikroskopischen Paläontologie gleichartig analysirter Gebirgsarten der Erde, mit specieller Rücksicht auf den Polycystinen-Mergel von Barbados. Abhandlungen der Koniglichen Akademie der Wissenschaften zu Berlin, 1875:1–226.

Goll, R.M., 1968. Classification and phylogeny of Cenozoic Trissocyclidae (Radiolaria) in the Pacific and Caribbean basins, Part 1. Journal of Paleontology, 42(6):1409–1432.

Haeckel, E., 1861. Fernere Abbildungen und Diagnosen neuer Gattungen und Arten von lebenden Radiolarien des Mittelmeeres. Monatsberichte der Königlich Preußischen Akademie der Wissenschaften zu Berlin, 1860:835–845.

Haeckel, E., 1862. Die Radiolarien (Rhizopoda radiaria) : eine Monographie: Berlin (G. Reimer). **https://www.biodiversitylibrary.org/item/40590**

Haeckel, E., 1882. Entwurf eines Radiolarien-Systems auf Grund von Studien der Challenger-Radiolarien. Jenaische Zeitschrift für Naturwissenschaft herausgegeben von der medizinisch-naturwissenschaftlichen Gesellschaft zu Jena, 15:418–472.

Haeckel, E., 1887. Report on the Radiolaria collected by H.M.S. Challenger during the years 1873–1876. Zoology, 18. **https://www.gutenberg.org/ebooks/44527**

Johnson, D.A., 1974. Radiolaria from the eastern Indian Ocean, DSDP Leg 22. In von der Borch, C.C., Sclater, J.G., et al., Initial Reports of the Deep Sea Drilling Project. 22: Washington, DC (US Government Printing Office), 521–574. **https://doi.org/10.2973/dsdp.proc.22.125.1974**

Jørgensen, E., 1905. The protist plankton and diatoms in bottom samples. In Nordgaard, O., Hydrographical and Biological investigations in Norwegian Fiords. VII. Radiolaria: Bergen, Norway (Bergen Museum Skrifter), 114–142.

Kamikuri, S., 2017. Late Neogene radiolarian biostratigraphy of the eastern North Pacific ODP Sites 1020/1021. Paleontological Research, 21(3):230–254. **https://doi.org/10.2517/2016PR027**

Kamikuri, S., 2019a. Middle to Late Miocene radiolarians from ODP Site 1021 in the eastern North Pacific. Bulletin of the Geological Survey of Japan, 70(1–2):163–194. **https://doi.org/10.9795/bullgsj.70.163**

Kamikuri, S., 2019b. Radiolarian assemblages from the lower to middle Miocene at IODP Site U1335 in the eastern equatorial Pacific. Bulletin of the geological Survey of Japan, 70(1–2):137–161. **https://doi.org/10.9795/bullgsj.70.137**

Kamikuri, S., 2022. Tropical radiolarian biostratigraphy from the Early to Late Miocene at ODP Site 714 in the Tropical Indian Ocean. Paleontological Research, 26(2):187–212. **https://doi.org/10.2517/PR200017**

Kamikuri, S., Moore, T.C., Ogane, K., Suzuki, N., Pälike, H., and Nishi, H., 2012. Early Eocene to early Miocene radiolarian biostratigraphy for the low-latitude Pacific Ocean. Stratigraphy, 9(1):77–108. **https://www.micropress.org/microaccess/stratigraphy/issue-292/article-1785**

Kamikuri, S., Motoyama, I., Nishi, H., and Iwai, M., 2009. Evolution of Eastern Pacific Warm Pool and upwelling processes since the middle Miocene based on analysis of radiolarian assemblages: response to Indonesian and Central American seaways. Palaeogeography, Palaeoclimatology, Palaeoecology, 280(3–4):469–479. **https://doi.org/10.1016/j.palaeo.2009.06.034**

Kamikuri, S., Nishi, H., Motoyama, I., and Saito, S., 2004. Middle Miocene to Pleistocene radiolarian biostratigraphy in the Northwest Pacific Ocean, ODP Leg 186. Island Arc, 13(1):191–226. **https://doi.org/10.1111/j.1440-1738.2003.00421.x**

Kling, S.A., 1971. Radiolaria, Leg 6 of the Deep Sea Drilling Project. In Fischer, A.G., et al., Initial Reports of the Deep Sea Drilling Project. 6: Washington, DC (US Government Printing Office), 1069–1117. **https://doi.org/10.2973/dsdp.proc.6.134.1971**

Kling, S.A., 1973. Radiolaria from the eastern North Pacific Deep Sea Drilling Project, Leg 18. In Kulm, L.D., von Huene, R., et al., Initial Reports of the Deep Sea Drilling Project. 18: Washington, DC (US Government Printing Office), 617–671. **https://doi.org/10.2973/dsdp.proc.18.116.1973**

Kruglikova S, B., 1974. Kharakternye vidy radiolayriy v donnykh osadkakh voreal'noi zony Tikhogo okeana. Mikropaleontologiya Okeanov i Morey, Akademiya Nauk SSSR, 85:187–196. **https://cir.nii.ac.jp/crid/1573668925703911680**

Lazarus, D., Faust, K., and Popova-Goll, I., 2005. New species of prunoid radiolarians from the Antarctic Neogene. Journal of Micropalaeontology, 24:97–121. **https://doi.org/10.1144/jm.24.2.97**

Ling, H.Y., 1975. Radiolaria: Leg 31 of the Deep Sea Drilling Project. In Karig, D.E., Ingle, J.C., Jr., et al., Initial Reports of the Deep Sea Drilling Project. 31: Washington, DC (US Government Printing Office), 703–761. **http://hdl.handle.net/10.2973/dsdp.proc.31.137.1975**

Martin, G.C., 1904. Protozoa. Maryland Geological Survey, 1904:447–459.

Martini, E., 1971. Standard Tertiary and Quaternary calcareous nannoplankton zonation. Proceedings of the Second Planktonic Conference, Roma, 1970:739–785.

Matsuzaki, K.M., 2021. Lower Pliocene and Upper Miocene collodarians and spumellarians (polycystine radiolarians) from the northwestern Pacific Ocean (ODP Site 1208). Revue de Micropaléontologie, 72:100515. **https://doi.org/10.1016/j.revmic.2021.100515**

Matsuzaki, K.M., and Itaki, T., 2019. Late Miocene polycystine radiolarians of the Japan Sea (IODP Exp. 346 Site U1425). Bulletin of the geological Survey of Japan, 70(1/2):195–209. **https://www.gsj.jp/data/bulletin/70_01_12.pdf**

Matsuzaki, K.M., Nishi, H., Hayashi, H., Suzuki, N., Gyawali, B.R., Ikehara, M., Tanaka, T., and Takashima, R., 2014. Radiolarian biostratigraphic scheme and stable oxygen isotope stratigraphy in southern Japan (IODP Expedition 315 Site C0001). Newsletters on Stratigraphy, 47(1):107–130. **https://doi.org/10.1127/0078-0421/2014/0044**

Matsuzaki, K.M., Suzuki, N., and Nishi, H., 2015. Middle to Upper Pleistocene polycystine radiolarians from Hole 902-C9001C, Northwestern Pacific. Paleontological Research, 19(s1):1–77. **https://doi.org/10.2517/2015PR003**

Moore, T.C., 1971. Radiolaria. In Tracey, J.I., Jr., et al., Initial Reports of the Deep Sea Drilling Project. 8: Washington, DC (US Government Printing Office), 727–775. **https://doi.org/10.2973/dsdp.proc.8.112.1971**

Moore, T.C., Jr., 1972. Mid-Tertiary evolution of the radiolarian genus Calocycletta. Micropaleontology, 18(2):144–152. **https://doi.org/10.2307/1484991**

Motoyama, I., 1996. Late Neogene radiolarian biostratigraphy in the subarctic Northwest Pacific. Micropaleontology, 42(3):221–262. **https://doi.org/10.2307/1485874**

Müller, J., 1859. Über die Thalassicollen, Polycystinen und Acanthometren des Mittelmeeres. Abhandlungen Koniglichen Akademie der Wissenschaften zu Berlin, 1858:1–62.

Nakaseko, K., 1955. Miocene radiolarian fossil assemblage from the southern Toyama Prefecture in Japan. Science Reports, South and North College, Osaka University, 4:65–127.

Nakaseko, K., 1963. Neogene Cyrtoidea (Radiolaria) from the Isozaki Formation in Ibaraki Prefecture, Japan. Science Reports, College of General Education, Osaka University, 12:165–198.

Nakaseko, K., 1971. On some species of the genus Thecosphaera from the Neogene formations, Japan. Science Reports, College of General Education, Osaka University, 20(2):59–66.

Nigrini, C., and Lombari, G., 1984. A Guide to Miocene Radiolaria. Special Publication - Cushman Foundation for Foraminiferal Research, 22.

Nigrini, C.A., Sanfilippo, A., and Moore, T.J., Jr., 2006. Cenozoic radiolarian biostratigraphy: a magnetobiostratigraphic chronology of Cenozoic sequences from ODP Sites 1218, 1219, and 1220, equatorial Pacific. In Wilson, P.A., Lyle, M., and Firth, J.V., Proceedings of the Ocean Drilling Program, Scientific Results. 199: College Station, TX (Ocean Drilling Program). **https://doi.org/10.2973/odp.proc.sr.199.225.2006**

O'Connor, B., 1997. New Radiolaria from the Oligocene and Early Miocene of Northland, New Zealand. Micropaleontology, 43(1):63–100. **https://doi.org/10.2307/1485923**

O'Dogherty, L., Caulet, J.-P., Dumitrica, P., and Suzuki, N., 2021. Catalogue of Cenozoic radiolarian genera (Class Polycystinea). Geodiversitas, 43(21):709–1185. **https://doi.org/10.5252/geodiversitas2021v43a21**

Palmer, A.A., 1981. Biostratigraphic age control for paleo-oceanographic study of Atlantic margin Miocene diatomites from planktonic siliceous microfossils. AAPG Bulletin, 65(9):1668.

Petrushevskaya, M.G., 1975. Cenozoic radiolarians of the Antarctic, Leg 29, DSDP. In Kennett, J.P., Houtz, R.E., et al., Initial Reports of the Deep Sea Drilling Project. 29: Washington, DC (US Government Printing Office), 541–675. **https://doi.org/10.2973/dsdp.proc.29.114.1975**

Petrushevskaya, M.G., and Kozlova, G.E., 1972. Radiolaria: Leg 14, Deep Sea Drilling Project. In Hayes, D.E., Pimm, A.C., et al., Initial Reports of the Deep Sea Drilling Project. 14: Washington, DC (US Government Printing Office), 495–648. **https://doi.org/10.2973/dsdp.proc.14.116.1972**

Renaudie, J., and Lazarus, D.B., 2012. New species of Neogene radiolarians from the Southern Ocean. Journal of Micropalaeontology, 31(1):29–52. **https://doi.org/10.1144/0262-821X10-026**

Renaudie, J., and Lazarus, D.B., 2016. New species of Neogene radiolarians from the Southern Ocean – part IV. Journal of Micropalaeontology, 35(1):26–53. **https://doi.org/10.1144/jmpaleo2014-026**

Riedel, W.R., 1954. The age of the sediment collected at Challenger (1875) Station 225 and the distribution of Ethmodiscus rex (Rattray). Deep Sea Research (1953), 1(3):170–175. **https://doi.org/10.1016/0146-6313(54)90046-5**

Riedel, W.R., 1959. Oligocene and Lower Miocene Radiolaria in tropical Pacific sediments. Micropaleontology, 5(3):285–302. **https://doi.org/10.2307/1484421**

Riedel, W.R., and Holm, E.A., 1957. Radiolaria. In Hedgpeth, J.W. (Ed.), Treatise on Marine Ecology and Paleoecology. Geological Society of America Memoir, 67V1: 0. **https://doi.org/10.1130/MEM67V1-p1069**

Riedel, W.R., and Sanfilippo, A., 1970. Radiolaria, Leg 4, Deep Sea Drilling Project. In Bader, R.G., et al., Initial Reports of the Deep Sea Drilling Project. 4: Washington, DC (US Government Printing Office), 503–575. **https://doi.org/10.2973/dsdp.proc.4.124.1970**

Riedel, W.R., and Sanfilippo, A., 1971. Cenozoic Radiolaria from the western tropical Pacific, Leg 7. In Winterer, E.L., et al., Initial Reports of the Deep Sea Drilling Project. 7: Washington, DC (US Government Printing Office), 1529–1672. **https://doi.org/10.2973/dsdp.proc.7.132.1971**

Riedel, W.R., and Sanfilippo, A., 1978. Stratigraphy and evolution of tropical Cenozoic radiolarians. Micropaleontology, 24(1):61–96. **https://doi.org/10.2307/1485420**

Riedel, W.R., and Sanfilippo, A., 1986. Morphological characters for a natural classification of Cenozoic Radiolaria, reflecting phylogenies. Marine Micropaleontology, 11(1–3):151–170. **https://doi.org/10.1016/0377-8398(86)90011-3**

Rosenthal, Y., Holbourn, A.E., Kulhanek, D.K., Aiello, I.W., Babila, T.L., Bayon, G., Beaufort, L., Bova, S.C., Chun, J.-H., Haowen, D., Drury, A.J., Dunkley Jones, T., Eichler, P.P.B., Fernando, A.G.S., Gibson, K.A., Hatfield, R.G., Johnson, D.L., Kumagai, Y., Tiegang, L., Linsley, B.K., Meinicke, N., Mountain, G.S., Opdyke, B.N., Pearson, P.N., Poole, C.R., Ravelo, A.C., Sagawa, T., Schmitt, A., Wurtzel, J.B., Jian, X., Yamamoto, M., and Zhang, Y.G., 2018a. Expedition 363 methods. In Rosenthal, Y., Holbourn, A.E., Kulhanek, D.K., and the Expedition 363 Scientists, Western Pacific Warm Pool. Proceedings of the International Ocean Discovery Program, 363: College Station, TX (International Ocean Discovery Program). **https://doi.org/10.14379/iodp.proc.363.102.2018**

Rosenthal, Y., Holbourn, A.E., Kulhanek, D.K., Aiello, I.W., Babila, T.L., Bayon, G., Beaufort, L., Bova, S.C., Chun, J.-H., Haowen, D., Drury, A.J., Dunkley Jones, T., Eichler, P.P.B., Fernando, A.G.S., Gibson, K.A., Hatfield, R.G., Johnson, D.L., Kumagai, Y., Tiegang, L., Linsley, B.K., Meinicke, N., Mountain, G.S., Opdyke, B.N., Pearson, P.N., Poole, C.R., Ravelo, A.C., Sagawa, T., Schmitt, A., Wurtzel, J.B., Jian, X., Yamamoto, M., and Zhang, Y.G., 2018b. Site U1490. In Rosenthal, Y., Holbourn, A.E., Kulhanek, D.K., and the Expedition 363 Scientists, Western Pacific Warm Pool. Proceedings of the International Ocean Discovery Program, 363: College Station, TX (International Ocean Discovery Program). **https://doi.org/10.14379/iodp.proc.363.111.2018**

Sakai, T., 1980. Radiolarians from Sites 434, 435, and 436, Northwest Pacific, Leg 56, Deep Sea Drilling Project. In Scientific Party (Co-Chiefs: von Huene, R., Nasu, N.), Initial Reports of the Deep Sea Drilling Project. 56: Washington, DC (US Government Printing Office), 695–733. **https://doi.org/10.2973/dsdp.proc.5657.119.1980**

Sanfilippo, A., Burckle, L.H., Martini, E., and Riedel, W.R., 1973. Radiolarians, diatoms, silicoflagellates and calcareous nannofossils in the Mediterranean Neogene. Micropaleontology, 19(2):209–234. **https://doi.org/10.2307/1485164**

Sanfilippo, A., and Nigrini, C., 1998. Code numbers for Cenozoic low latitude radiolarian biostratigraphic zones and GPTS conversion tables. Marine Micropaleontology, 33(1):109–156. **https://doi.org/10.1016/S0377-8398(97)00030-3**

Sanfilippo, A., and Riedel, W., 1980. A revised generic and suprageneric classification of the artiscins (Radiolaria). Journal of Paleontology, 54(5):1008–1011. **http://www.jstor.org/stable/1304365**

Sanfilippo, A., and Riedel, W.R., 1970. Post-Eocene "closed" theoperid radiolarians. Micropaleontology, 16(4):446–462. **https://doi.org/10.2307/1485072**

Sanfilippo, A., and Riedel, W.R., 1992. The origin and evolution of Pterocorythidae (Radiolaria): a Cenozoic phylogenetic study. Micropaleontology, 38(1):1–36. **https://doi.org/10.2307/1485841**

Sanfilippo, A., Westberg-Smith, M.J., and Riedel, W.R., 1985. Cenozoic radiolaria. In Bolli, H.M., Saunders, J.B., and Perch-Nielsen, K., Plankton Stratigraphy (Volume 2): Radiolaria, Diatoms, Silicoflagellates, Dinoflagellates, and Ichthyoliths. Cambridge, UK (Cambridge University Press), 631–712.

Stöhr, E., 1880. Die Radiolarienfauna der Tripoli von Grotte, Provinz Girgenti in Sicilien. Palaeontographica, 26(4):69–124.

Sugiyama, K., and Furutani, H., 1992. Middle Miocene radiolarians from the Oidawara Formation, Mizunami Group, Gifu Prefecture, central Japan. Bulletin of the Mizunami Fossil Museum, 19:199–213.

Suzuki, N., Ogane, K., Aita, Y., Sakai, T. and Lazarus, D., 2009. Reexamination of Ehrenberg's Neogene radiolarian collections and its impact on taxonomic stability. National Museum of Nature and Science Monograph, 40:87–96.

Tan, Z., and Su, X., 1982. Studies on the Radiolaria in sediments of the East China Sea (continental shelf). Studia Marina Sinica, 19:129–216.

Vinassa de Regny, P.E., 1900. Radiolaria Miocenici Italiani. Memorie della Regia Accademia delle Scienze dell'instituto di Bologna, 5:565–595.

Zhang, L., and Suzuki, N., 2017. Taxonomy and species diversity of Holocene pylonioid radiolarians from surface sediments of the northeastern Indian Ocean. Palaeontologia Electronica, 20:20.23.48A. **https://doi.org/10.26879/718**

Appendix

Taxonomic notes

We define brief synonymies for the encountered radiolarian species.

Order COLLODARIA Haeckel, 1882
Genus *Polysolenia* Ehrenberg, 1861

***Polysolenia spinosa* (Haeckel, 1861) sensu Matsuzaki (2021)**
(Plate P1, figures 8, 11)

Collosphaera spinosa n. sp. Haeckel, 1861, p. 845.
Acrosphaera echinoides n. sp. Haeckel, 1887, p. 100.
Polyselonia spinosa (Haeckel); Matsuzaki et al., 2014, pl. 1, figs. 1, 2.
Polyselonia spinosa (Haeckel) group Kamikuri, 2019b, pl. 1, figs. 8, 10.
Polysolenia spinosa (Haeckel, 1861) sensu lato Matsuzaki, 2021, p. 2-2, pl. 1, fig. 2 (only).

***Polysolenia* sp. A**
(Plate P1, figure 10)

Remarks. It differs from *Polysolenia spinosa* (Haeckel, 1861) sensu lato by having highly variable pore sizes.

***Polysolenia glebulenta* (Bjørklund and Goll, 1979)**
(Plate P1, figure 9)

Collosphaera glebulenta n. sp. Bjørklund and Goll, 1979, pp. 1316, 1317, pl. 2, figs. 9–25.
Collosphaera glebulenta Bjørklund and Goll; Boltovskoy and Jankilevich, 1985, pl. 1, fig. 4.

Genus *Siphonosphaera* Müller, 1859

***Siphonosphaera* sp. A**
(Plate P1, figure 13)

Genus *Disolenia* Ehrenberg, 1861

***Disolenia* sp. A**
(Plate P1, figure 14)

***Disolenia* spp.**
(Plate P1, figures 15, 16)

Order SPUMELLARIA Ehrenberg, 1876
Genus *Spongasteriscus* Haeckel, 1862

***Spongasteriscus marylandicus* Martin, 1904**
(Plate P1, figures 1, 2)

Spongasteriscus marylandicus n. sp. Martin, 1904, p. 453, pl. 130, fig. 10.
Histiastrum martinianum n. sp. Carnevale, 1908, pp. 26, 27, pl. 4, fig. 11.
Spongasteriscus spp. Petrushevskaya and Kozlova, 1972, p. 529, pl. 20, fig. 12; pl. 21, figs. 6, 7.
Histiastrum martinianum Carnevale group Sanfilippo et al., 1973, p. 217, pl. 2, figs. 7, 8.

***Stephanastrum* sp. A**
(Plate P1, figure 12)

Spongaster sp. A Kamikuri, 2019a, pl. 21, fig. 13.

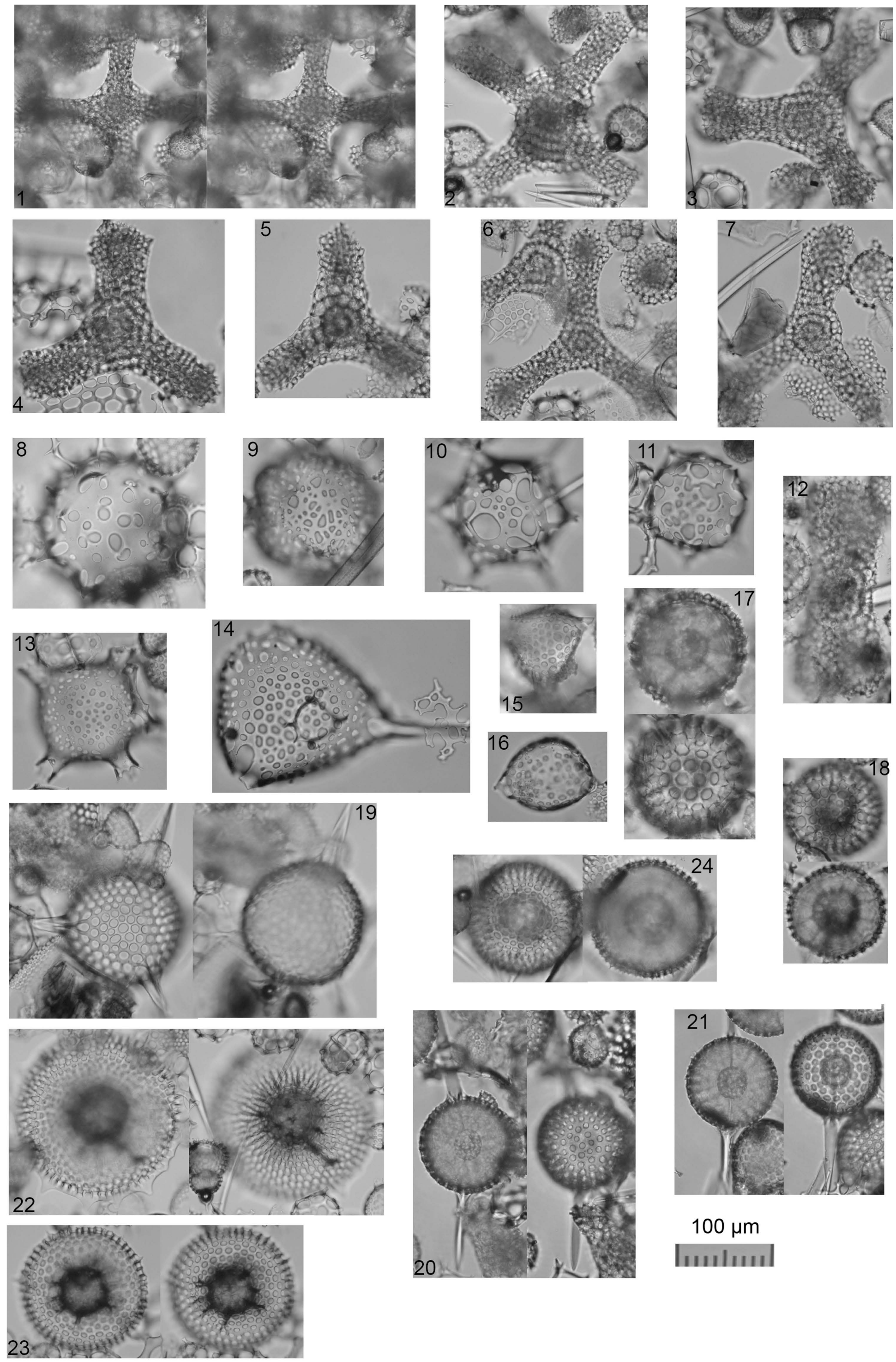

Plate P1. Radiolarians, Hole U1490A. 1, 2. *Spongasteriscus marylandicus* (Martin) (41X-CC). 3–7. *Dictyocoryne malagaense* (Campbell and Clark) (3, 4, 6, 7: 23H-CC; 5. 25H-CC). 8, 11. *Polysolenia spinosa* group (Haeckel) (8: 23H-CC; 11: 20H-CC). 9. *Polysolenia glebulenta* Bjørklund and Goll (31F-CC). 10. *Polysolenia* sp. A (20H-CC). 12. *Stephanastrum* sp. A (35X-CC). 13. *Siphonosphaera* sp. A (27H-CC). 14. *Disolenia* sp. A (20H-CC). 15, 16. *Disolenia* spp. (23H-CC). 17. *Haliomma* sp. A (41X-CC). 18. *Eccentrodiscus* sp. A (41X-CC). 19. *Haliphormis aculeata* (Campbell and Clark) (35X-CC). 20, 21. *Stylatractona* sp. A (41X-CC), 22. *Heliodiscus grottensis* Stöhr (25H-CC). 23. *Heliodiscus* sp. A (25H-CC). 24. *Haliomma dedondoensis* group (Nakasekoi) (35X-CC).

Genus *Dictyocoryne* Ehrenberg, 1861

***Dictyocoryne malagaense* (Campbell and Clark, 1944) group**
(Plate P1, figures 3–7)

Rhopalodictyum (Rhopalodictya) malagaense n. sp. Campbell and Clark, 1944, p. 29, pl. 4, figs. 4, 5.
Dictyocoryne malagaense Campbell and Clark; Kamikuri 2019b, pl. 9, fig. 5; Kamikuri, 2019a, pl. 19, figs. 1, 2.
Dictyocoryne malagaense (Campbell and Clark, 1944) group Matsuzaki, 2021, figs. 14, 15, 23.

Genus *Thecosphaera* Haeckel, 1882

***Thecosphaera* sp. A**
(Plate P1, figure 17)

***Thecosphaera dedoensis* Nakaseko, 1971 group**
(Plate P1, figure 24)

Thecosphaera dedoensis n. sp. Nakaseko, 1971, p. 61, pl. 2, figs. 2a, 2b.
Thecosphaera dedoensis Nakaseko; Motoyama, 1996, pl. 2, fig. 2; Kamikuri, 2019a, pl. 13, figs. 1–8.

Remarks. The morphology of *T. dedoensis* in Kamikuri (2019a) differs slightly from the holotype by having more numerous pores on the Equator. Thus, we propose here the name for such morphotypes as *T. dedoensis* group.

Genus *Excentrodiscus* Hollande and Enjumet, 1960

***Excentrodiscus planangulus* Renaudie and Lazarus, 2016**
(Plate P1, figure 18)

Excentrodiscus planangulus n. sp. Renaudie and Lazarus, 2016, pp. 31–33, pl. 2, figs. 1A-3, A-6.

Genus *Hexastylus* Haeckel, 1882

***Hexastylus aculeata* (Campbell and Clark, 1944)**
(Plate P1, figure 19)

Staurolonche (Staurolonchantha) aculeata Campbell and Clark, 1944, p. 13, pl. 2, figs. 2, 3.
Hexastylus aculeata (Campbell and Clark); Kamikuri, 2019a, pl. 12, figs. 3a, 3b.

Genus *Stylatractona* Haeckel, 1887

***Stylatractona* sp. A**
(Plate P1, figures 20, 21)

Genus *Heliodiscus* Haeckel, 1862

***Heliodiscus grottensis* Stöhr, 1880**
(Plate P1, figure 22)

Heliodiscus grottensis n. sp. Stöhr, 1880, p. 89, pl. 1, fig. 13.
Heliodiscus (Heliodiscetta) siculus Stoehr; Haeckel, 1887, p. 446.
Heliodrymus (Heliocladus) grottensis (Stoehr); Haeckel, 1887 p. 451.

***Heliodiscus* sp. A**
(Plate P1, figure 23)

Genus *Didymocyrtis* Haeckel, 1862

***Didymocyrtis prismatica* (Haeckel, 1887)**
(Plate P2, figures 1, 2, 4)

Pipettella prismatica n. sp. Haeckel, 1887, p. 305, pl. 39, fig. 6.
Pipettella prismatica Haeckel; Riedel, 1959, pp. 287, 288, pl. 1, fig. 1.

Cannartus prismaticus (Haeckel); Riedel and Sanfilippo, 1970, p. 520, pl. 15, fig. 1; Ling, 1975, p. 717, pl. 2, figs. 7, 8.
Didymocyrtis prismatica (Haeckel); Nigrini and Lombari, 1984, S45, S46, pl. 6, figs. 3a, 3b; Kamikuri et al., 2009, fig. 9A; Kamikuri, 2019b, pl. 6, figs. 4, 5.

Didymocyrtis tubaria (Haeckel, 1887)
(Plate **P2**, figures 3, 5)

Pipettaria tubaria n. sp. Haeckel, 1887, p. 339, pl. 39, fig. 15.
Cannartus tubarius (Haeckel); Riedel and Sanfilippo, 1970, p. 520, pl. 15, fig. 2; Sakai, 1980, p. 707, pl. 5, figs. 11a, 11b.
Didymocyrtis tubaria (Haeckel); Sanfilippo et al., 1985, p. 659, fig. 8.2; Sugiyama and Furutani, 1992, p. 201, pl. 16, fig. 1; Kamikuri et al., 2009, fig. 9B; Kamikuri, 2019b, pl. 6, figs. 6, 7.

Didymocyrtis bassanii (Carnevale, 1908)
(Plate **P2**, figures 6–8)

Cannartidium bassanii n. sp. Carnevale, 1908, p. 21, pl. 3, fig. 12.
Cannartus bassanii (Carnevale); Sanfilippo et al., 1973, p. 216, pl. 1, figs. 1–3.
Didymocyrtis bassanii (Carnevale); O'Connor, 1997, p. 112; Nigrini et al., 2006, p. 32, pl. P1, fig. 5; Kamikuri et al., 2009, fig. 9H; Kamikuri, 2019b, pl. 6, figs. 10, 12, 13.

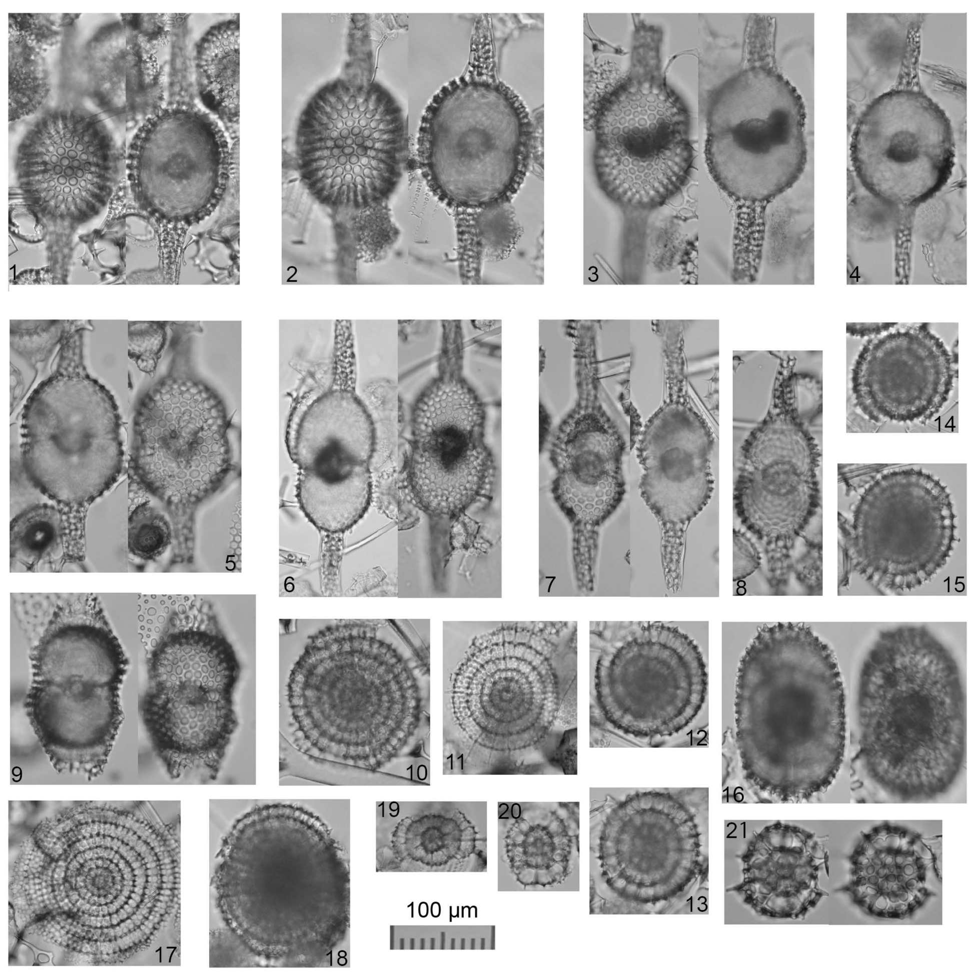

Plate P2. Radiolarians, Hole U1490A. 1, 2, 4. *Didymocyrtis prismatica* (Haeckel) (1, 2: 41X-CC; 4: 35X-CC). 3, 5. *Didymocyrtis tubaria* (Haeckel) (3: 27H-CC; 5: 31F-CC). 6–8. *Didymocyrtis bassanii* (Carnevale) (35X-CC), 9. *Didymocyrtis* cf. *laticonus* (Riedel) (23H-CC). 10. *Stylodictya* sp. A (35X-CC). 11. *Stylodictya tenuispina* group Jørgensen (35X-CC). 12–15. *Lithelius haeckelispiralis* Matsuzaki and Suzuki (31F-CC). 16. *Larcopyle buetschlii* Dreyer (23H-CC). 18. *Lithelius hayesi* (Chen) (41X-CC). 19. *Phorticium* sp. A. (35X-CC). 20, 21. *Phorticium* cf. *scitulum* Zhang and Suzuki (20: 25H-CC; 21: 23H-CC).

Didymocyrtis cf. _laticonus_ (Riedel, 1959)
(Plate **P2**, figure 9)

Cannartus laticonus n. sp. Riedel, 1959, pp. 291, 292, pl. 1, fig. 5.
Cannartus laticonus Riedel; Sakai, 1980, p. 705, pl. 3, figs. 7a, 7b, 8a, 8b.
Didymocyrtis laticonus (Riedel); Sanfilippo and Riedel, 1980, text-fig. 1e; Nigrini and Lombari, 1984, S53, S54, pl. 7, figs. 1a–1c; Sanfilippo et al., 1985, p. 658, figs. 8.5a, 8.5b; Kamikuri et al., 2009, fig. 9E; Kamikuri, 2019b, pl. 6, fig. 8.

Genus _Stylodictya_ Ehrenberg, 1846

Stylodictya tenuispina Jørgensen, 1905 group sensu Matsuzaki (2021)
(Plate **P2**, figures 11–17)

Stylodictya tenuispina n. sp. Jørgensen, 1905, pp. 118, 119, pl. 10, fig. 39.
Stylodictya validispina Jørgensen; Kruglikova, 1974, p. 191, pl. 2, fig. 6 (only).
Stylodictya tenuispina Jørgensen group Matsuzaki and Itaki, 2019, pl. 2, figs. 24–27; Matsuzaki, 2021, figs. 4.16–4.19.

Stylodictya sp. A
(Plate **P2**, figure 10)

Genus _Lithelius_ Haeckel, 1861

Lithelius hayesi (Lazarus et al., 2005)
(Plate **P2**, figure 18)

Prunopyle hayesi n. sp. Chen, 1975, p. 454, pl. 9, figs. 4, 5 (only).
Ommatodiscus haeckeli group Petrushevskaya, 1975, p. 572, pl. 32.
Larcopyle hayesi, Lazarus et al., 2005, p. 119, 120, pl. 11, figs. 1–8, 18–20.

Remarks. Specimens belonging to this species are characterized by well-pronounced whorl-arranged morphology although each whorl is thin. Thus, following the nomenclature in Matsuzaki et al. (2015), we propose to move such specimens into the Genus *Lithelius* Haeckel.

Lithelius haeckelispiralis Matsuzaki and Suzuki in Matsuzaki et al., 2015
(Plate **P2**, figures 12–15)

Lithelius spiralis n. sp. Haeckel, 1861, pp. 519, 520, pl. 27, figs. 6, 7.
Lithelius spiralis Haeckel; Tan and Su, 1982, p. 162, pl. 13, figs. 9–11.
Lithelius haeckelispiralis Matsuzaki and Suzuki nomen nov. Matsuzaki et al. 2015, pp. 37, 38, figs. 6.32, 6.33, 6.37.

Genus _Larcopyle_ Dreyer, 1889 sensu Zhang and Suzuki, 2017

Larcopyle buetschlii Dreyer, 1889 sensu lato
(Plate **P2**, figure 16)

Larcopyle buetschlii n. sp. Dreyer, 1889, pp. 124, 125, fig. 70.
Larcopyle buetschlii Dreyer; Matsuzaki et al. 2015, p. 33, figs. 6.21–6.28; Matsuzaki, 2021, figs. 6.2–6.6.

Genus _Phorticium_ sensu Zhang and Suzuki, 2017

Phorticium cf. _scitulum_ Zhang and Suzuki, 2017 sensu lato
(Plate **P2**, figures 20, 21)

Phorticium scitulum n. sp. Zhang and Suzuki, 2017, pp. 45, 46, figs. 26.1–26.23.
Phorticium aff. *scitulum* Zhang and Suzuki; Matsuzaki and Itaki, 2019, pl. 3, figs. 9, 10, 12, 13; Matsuzaki, 2021, figs. 5.4, 5.6, 5.8, 5.10–5.12, 5.16.

Phorticium sp. A
(Plate P2, figure 19)

Order NASSELLARIA Ehrenberg, 1876
Genus *Cyrtocapsella* Haeckel, 1887

Cyrtocapsella cornuta (Haeckel, 1887)
(Plate P3, figures 1, 2)

Theocapsa (Theocapsura) darwinii n. sp. Haeckel, 1887, p. 1431, pl. 66, fig. 12.

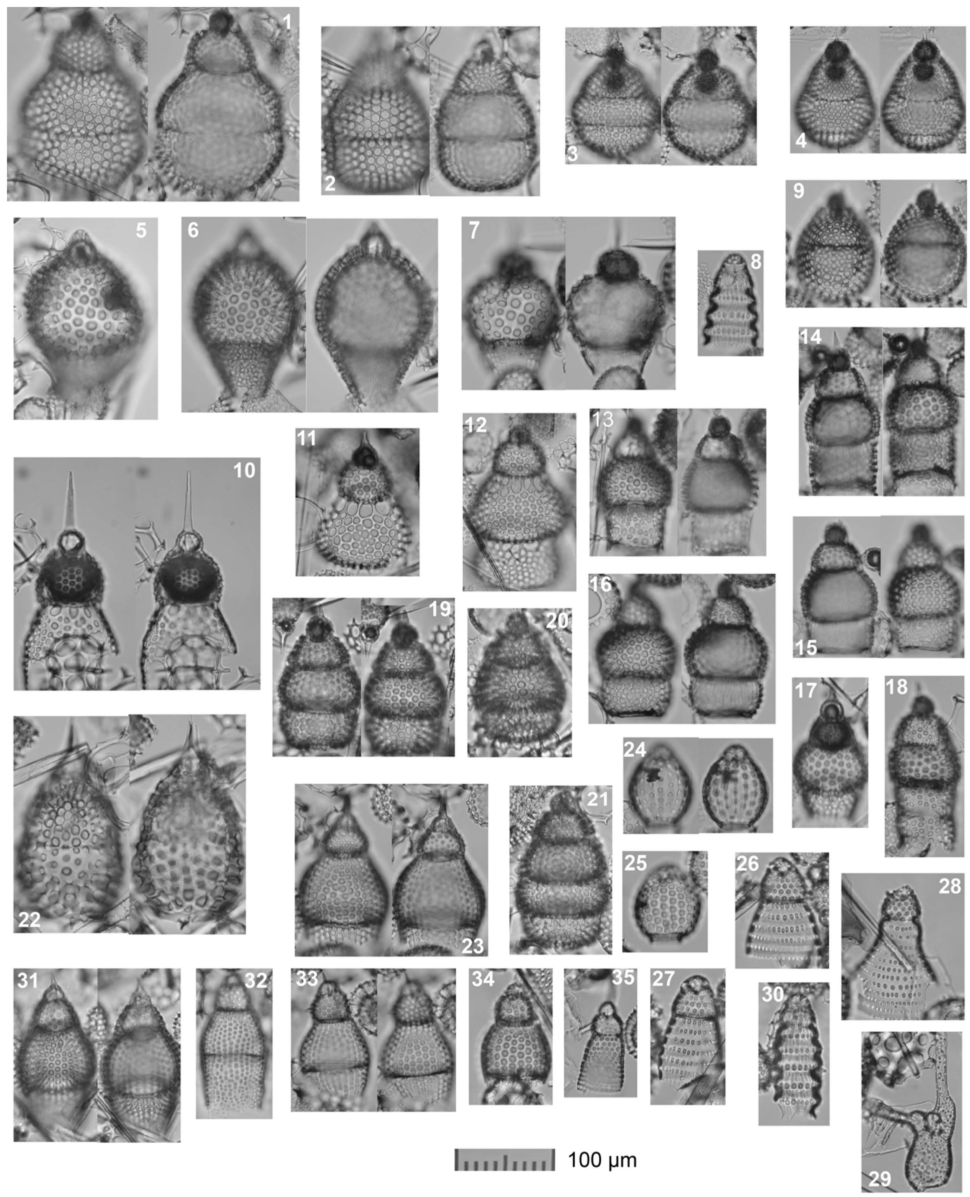

Plate P3. Radiolarians, Hole U1490A. 1, 2. *Cyrtocapsella cornuta* (Haeckel) (1: 27H-CC; 2: 31F-CC). 3, 4. *Cyrtocapsella tetrapera* (Haeckel) (35X-CC). 5, 6. *Theocorythium spongoconus* Kling (31F-CC). 7. *Theocorythium* sp. A (25H-CC). 8, 30. *Siphocampe nodosaria* Haeckel (8: 35X-CC; 30: 41H-CC). 9. *Cyrtocapsella elongata* (Nakaseko) (25H-CC). 10. *Stichocorys johnsoni* (Caulet) (23H-CC). 11, 12. *Stichocorys diaphanes* (Sanfilippo et al.) (35X-CC). 13. *Stichocorys wolffii* Haeckel (25H-CC). 14–18. *Stichocorys delmontensis* (Campbell and Clark) (14: 31F-CC; 15–17: 25H-CC; 18: 23H-CC). 19–21. *Lithocampe subligata* Stöhr (41X-CC). 22. *Lamprocyclas* sp. B sensu Kamikuri (31F-CC). 23, 31. *Phormocyrtis alexandrae* (41X-CC). 24. *Tricolocapsa* sp. A (41X-CC). 25. *Tricolocapsa* sp. B (41H-CC). 26, 27. *Siphocampe* sp. B (41X-CC). 28. *Siphocampe* sp. C (41X-CC). 29. *Pylobotrys disolenia* Haeckel (35X-CC). 32, 33. *Eucyrtidium cienkowskii* Haeckel (32: 27H-CC; 33: 35X-CC). 34. *Eucyrtidium* sp. aff. *inflatum* Kling (41X-CC). 35. *Artostrobus semazen* Renaudie and Lazarus (41X-CC).

Cyrtocapsa (Cyrtocapsella) cornuta n. sp. Haeckel, 1887, p. 1513, pl. 78, fig. 9.
Cyrtocapsella cornuta Haeckel; Riedel and Sanfilippo, 1970, p. 531, pl. 14, fig. 8.
Cyrtocapsella cornuta (Haeckel); Sakai, 1980, p. 709, pl. 8, figs. 8a, 8b; Sugiyama and Furutani, 1992, p. 208, pl. 17, fig. 11; Kamikuri et al., 2009, figs. 10X1, 10X2; Kamikuri, 2019b, pl. 10, figs. 5a, 5b; Kamikuri, 2019a, pl. 5, figs. 4a, 4b.

Cyrtocapsella tetrapera (Haeckel, 1887)
(Plate **P3**, figures 3, 4)

Cyrtocapsa (Cyrtocapsella) tetrapera n. sp. Haeckel, 1887, p. 1512, pl. 78, fig. 5.
Cyrtocapsa (Cyrtocapsella) cf. *tetrapera* Haeckel; Nakaseko, 1955, p. 119, pl. 11, figs. 7a, 7b.
Cyrtocapsella tetrapera Haeckel; Riedel and Sanfilippo, 1970, p. 530-531; Ling, 1975, p. 728, pl. 9, fig. 18; Sakai, 1980, p. 709, pl. 8, figs. 5, 6.
Lithocampe tetrapera (Haeckel); Petrushevskaya and Kozlova, 1972, p. 546, pl. 25, fig. 14.
Lithocampe radicula Ehrenberg; Suzuki et al., 2009, pl. 23, figs. 2a, 2b.
Cyrtocapsella tetrapera (Haeckel); Sanfilippo et al., 1973, p. 221, pl. 5, figs. 4–6; Nigrini and Lombari, 1984, N109, N110, pl. 23, fig. 5; Kamikuri et al., 2004, fig. 9.5; Kamikuri et al., 2009; figs. 10Z1, 10Z2; Kamikuri, 2019b, pl. 10, figs. 1a, 1b, 2a, 2b; Kamikuri, 2019a, pl. 5, fig. 5.

Cyrtocapsella elongata (Nakaseko, 1963)
(Plate **P3**, figure 9)

Theocapsa elongata n. sp. Nakaseko, 1963, p. 185, pl. 3, figs. 4, 5.
Cyrtocapsella elongata (Nakaseko); Sanfilippo and Riedel, 1970, p. 452, pl. 1, figs. 11, 12; Nigrini and Lombari, 1984, N105, N106, pl. 23, figs. 3a, 3b; Kamikuri, 2019b, pl. 10, figs. 3, 4; Kamikuri, 2019a, pl. 5, fig. 9.

Genus _Stichocorys_ Haeckel, 1882

Stichocorys johnsoni (Caulet, 1986)
(Plate **P3**, figure 10)

Theoperid, gen. et sp. indet. Johnson, 1974, pl. 8, fig. 1.
Stichocorys johnsoni n. sp. Caulet, 1986, p. 851, pl. 6, figs. 5, 6.
Stichocorys? *johnsoni* Caulet group Sugiyama and Furutani, 1992, p. 210, pl. 17, fig. 4.

Stichocorys delmontensis (Campbell and Clark, 1944)
(Plate **P3**, figures 14–18)

Eucyrtidium (Eucyrtis) delmontense n. sp. Campbell and Clark, 1944, p. 56, pl. 7, figs. 19, 20.
Stichocorys delmontensis (Campbell and Clark); Riedel and Sanfilippo, 1970, p. 530, pl. 14, fig. 6; Nigrini and Lombari, 1984, N129, N130, pl. 25, fig. 4; Sugiyama and Furutani, 1992, p. 210, pl. 14, fig. 6; Motoyama, 1996, pl. 5, fig. 3; Matsuzaki and Itaki, 2019, pl. 8, fig. 1; Kamikuri et al., 2009, fig. 10Q; Kamikuri, 2019b, pl. 10, figs. 8a, 8b; Kamikuri, 2019a, pl. 5, fig. 7.
Eucyrtidium lineatum (Ehrenberg); Suzuki et al., 2009, pl. 38, figs. 15a–16c.

Stichocorys diaphanes (Sanfilippo et al., 1973)
(Plate **P3**, figures 11, 12)

Calocyclas coronata n. sp. Carnevale, 1908, p. 33, pl. 4, fig. 24.
Eucyrtidium diaphanes Sanfilippo and Riedel nomen nov. Sanfilippo et al., 1973, p. 221, pl. 5, figs. 12–14; Nigrini and Lombari, 1984, N113, N114, pl. 23, fig. 7; Kamikuri et al., 2009, fig. 10M.
Stichocorys diaphanes (Sanfilippo and Riedel); Kamikuri, 2019b, pl. 10, fig. 17.

Stichocorys wolffii Haeckel, 1887
(Plate **P3**, figure 13)

Stichocorys wolffii n. sp. Haeckel, 1887, p. 1479, pl. 80, fig. 10.
Stichocorys wolffii Haeckel; Riedel and Holm, 1957, pp. 92, 93, pl. 4, figs. 6, 7; Sanfilippo et al., 1985, p. 682, figs. 23.3a, 23.3b; Kamikuri et al., 2009, fig. 10N; Kamikuri, 2019b, pl. 10, figs. 10a, 10b.

Genus *Lithocampe* Ehrenberg, 1846

***Lithocampe subligata* Stöhr**
(Plate **P3**, figures 19–21)

Lithocampe subligata Stöhr, 1880, p. 102, pl. 4, fig. 1.
Lithocampe subligata Stöhr group Petrushevskaya, 1975, p. 581, figs. 6–9, 12.

Genus *Eucyrtidium* Ehrenberg, 1846

***Eucyrtidium cienkowskii* Haeckel, 1887**
(Plate **P3**, figures 32, 33)

Eucyrtidium cienkowskii n. sp. Haeckel, 1887, p. 1493, pl. 80, fig. 9.
Eucyrtidium cienkowskii Haeckel group Sakai, 1980, p. 710, pl. 7, figs. 8a, 8b, 9, 10; Sugiyama and Furutani, 1992, p. 208, pl. 14, figs. 3, 4, pl. 17, fig. 6; Kamikuri, 2019a, pl. 4, figs. 9–11.

***Eucyrtidium* sp. aff. *inflatum* Kling, 1973**
(Plate **P3**, figure 34)

Genus *Phormocyrtis* Haeckel, 1887

***Phormocyrtis alexandrae* O'Connor, 1997**
(Plate **P3**, figures 23, 31)

Eucyrtidium sp. B Sakai, 1980, p. 710, pl. 7, figs. 7a, 7b.
Eucyrtidium sp. Sugiyama and Furutani, 1992, p. 209, pl. 14, fig. 2.
Phormocyrtis alexandrae n. sp. O'Connor, 1997, pp. 110, 111, pl. 2, figs. 9–12; pl. 6, figs. 1–4, 6.

Genus *Anthocyrtidium* Haeckel, 1882

***Anthocyrtidium achillis* Haeckel, 1887**
(Plate **P4**, figure 11)

Sethocorys achillis n. sp. Haeckel, 1887, p. 1301, pl. 62, fig. 8.
Anthocyrtidium achillis Haeckel; Caulet, 1979, p. 132, pl. 2, fig. 4.

***Anthocyrtidium* sp. A**
(Plate **P4**, figure 12)

Genus *Lamprocyclas* Haeckel, 1882

***Lamprocyclas* sp. B sensu Kamikuri, 2019b**
(Plate **P3**, figure 22)

Lamprocyclas sp. B Kamikuri, 2019b, pl. 14, figs. 4a, 4b.

Genus *Calocyclas* Ehrenberg, 1847

Remarks. Based on O'Dogherty et al. (2021), the genus *Calocycletta* Haeckel (1887) is a junior synonym of the genus *Calocyclas* Ehrenberg (1847). Thus, in this study we use the genus *Calocyclas* for species belonging to the genus *Calocycletta* Haeckel.

***Calocyclas costata* Riedel, 1959**
(Plate **P4**, figures 1, 2)

Anthocyrtium (Anthocyrturium) flosculus n. sp. Haeckel, 1887, pp. 1277, 1278, pl. 62, fig. 19.
Calocyclas virginis Haeckel; Riedel, 1959, pp. 90–92, pl. 4, fig. 5.
Calocyclas costata n. sp. Riedel, 1959, pp. 296, 298, pl. 2, fig. 9.
Calocycletta costata (Riedel); Riedel and Sanfilippo, 1970, p. 535, pl. 14. fig. 12.

Calocyclas serrata (Moore, 1972)
(Plate P4, figure 3)

Calocycletta cf. *virginis* Haeckel; Riedel and Sanfilippo, 1970, pl. 14, fig. 11.
Calocycletta serrata n. sp. Moore, 1972, pp. 148, 150, pl. 2, figs. 1–3.
Calocycletta serrata Moore; Nigrini and Lombari, 1984, N159, N160, pl. 29, figs. 1a–1c; Riedel and Sanfilippo, 1986, pl. 6, figs. 12, 13; Palmer, 1981, pl. 1, fig. 3.

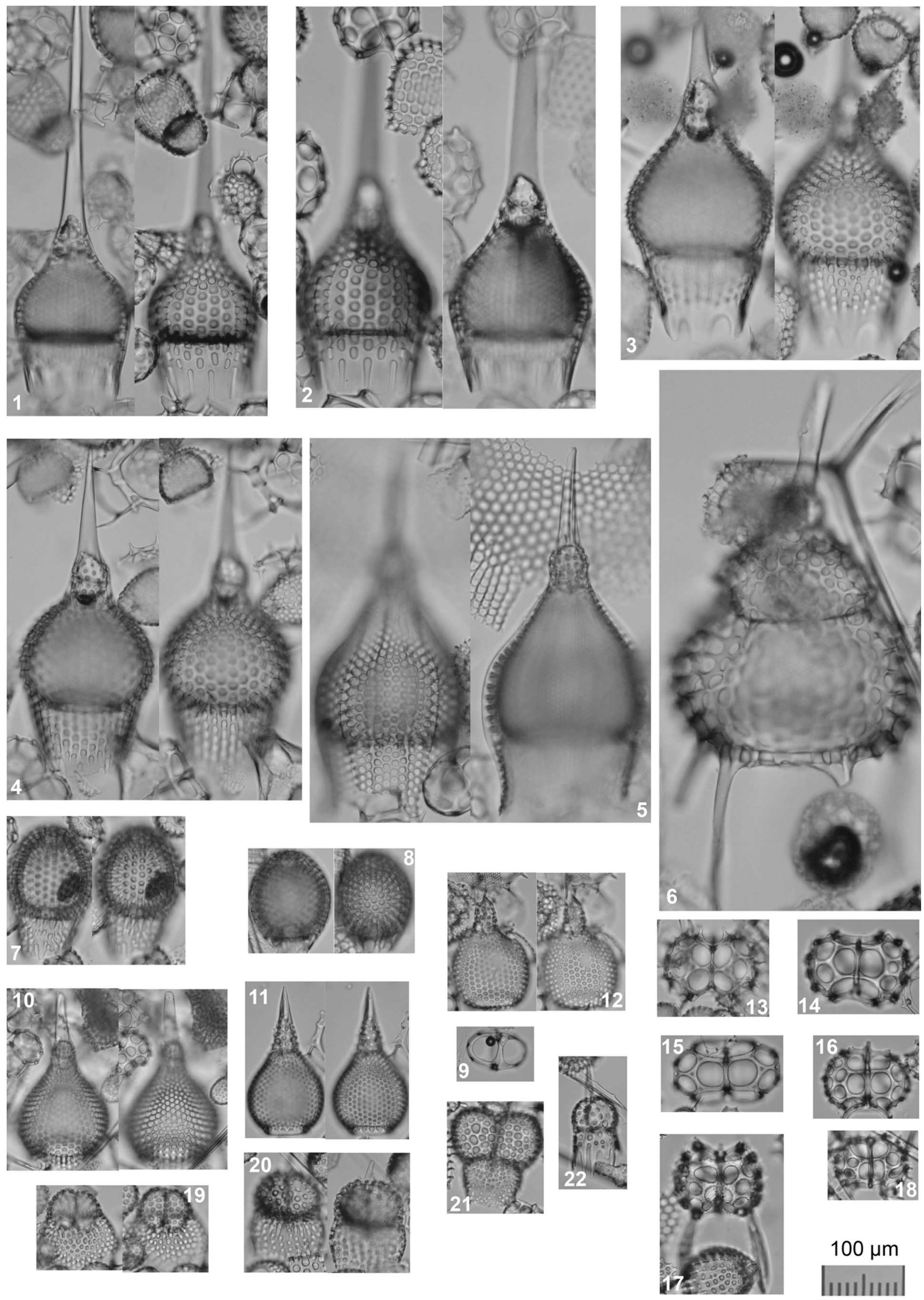

Plate P4. Radiolarians, Hole U1490A. 1, 2. *Calocyclas costata* Riedel (25H-CC). 3. *Calocyclas serrata* (Moore) (34X-CC). 4. *Calocyclas virginis* Haeckel (35X-CC). 5. *Theocorythium annosa* (Riedel) (39X-CC). 6. *Artophormis gracilis* (Riedel) (39X-CC). 7, 8. *Carpocanopsis cingulata* (Riedel and Sanfilippo) (26H-CC). 9. *Trissocyclus stauroporus* (Haeckel, 1887) (26H-CC). 10. *Calocyclas caepa* Moore (31F-CC). 11. *Anthocyrtidium achillis* Haeckel (35X-CC). 12. *Anthocyrtidium* sp. A (35X-CC). 13. *Tholospyris mammillaris* (Haeckel) (27H-CC). 14–18. *Tholospyris* spp. (14: 23H-C; 15, 16, 18: 25H-CC; 17: 41X-CC). 19, 20. *Dendrospyris* aff. *bursa* sensu Sanfilippo and Riedel (19: 31F-CC; 20: 25H-CC). 21. *Dendrospyris* sp. A (41X-CC). 22. *Dendrospyris* sp. B (41X-CC).

Remarks. *Calocyclas serrata* can be distinguished from other *Calocyclas* species by the presence of well-pronounced undulated wavy feet on the bottom of the abdomen.

Calocyclas virginis Haeckel, 1887
(Plate **P4**, figure 4)

Calocyclas (Calocycletta) virginis n. sp. Haeckel, 1887, pp. 1381, 1382, pl. 74, fig. 4.
Calocyclas virginis Haeckel; Riedel, 1954, pp. 172, 173.
Calocycletta virginis (Haeckel); Sanfilippo et al., 1973, p. 226, pl. 6, fig. 11; Sakai, 1980, p. 711, pl. 10, figs. 5a, 5b; Sanfilippo et al., 1985, p. 693, figs. 28.1a, 28.1b.

Calocyclas caepa (Moore, 1972)
(Plate **P4**, figure 10)

Calocycletta caepa n. sp. Moore, 1972, p. 150, pl. 2, figs. 4–7.
Calocycletta caepa Moore; Nigrini and Lombari, 1984, N153, N154, pl. 28, figs. 1a–1d; Sanfilippo et al., 1985, figs. 28.5a, 28.5b.

Calocyclas cladara (Sanfilippo and Riedel, 1992)

Calocycletta (Calocycletta) cladara Sanfilippo and Riedel, 1992, p. 30, pl. 2, figs. 12–16.

Genus _Theocorythium_ Haeckel, 1887

Remarks. According to O'Dogherty et al. (2021), the genus *Theocyrtis* Haeckel, 1887 is a junior synonym of the genus *Theocorythium* Haeckel, 1887. Thus, in this study we refer to the genus *Theocorythium* Haeckel, 1887 all specimens belonging to the genus *Theocyrtis* Haeckel, 1887.

Theocorythium spongoconus (Kling, 1971)
(Plate **P3**, figures 5, 6)

Theocorys spongoconus n. sp. Kling, 1971, p. 1087, pl. 5, fig. 6.
Theocorys spongoconum Kling; Sakai, 1980, p. 711, pl. 8, fig. 14.
Theocorys spongoconus Kling; Nigrini et al., 2006, pp. 48, 49, pl. P4, figs. 19–21.

Theocorythium sp. A
(Plate **P3**, figure 7)

Theocorythium annosa (Riedel, 1959)
(Plate **P4**, figure 5)

Phormocyrtis annosa n. sp. Riedel, 1959, p. 294, pl. 2, fig. 7.
Theocyrtis annosa (Riedel); Riedel and Sanfilippo, 1970, p. 535, pl. 15, fig. 9; Nigrini et al., 2006, p. 50, pl. P5, fig. 14; Kamikuri et al., 2012, pl. 2, fig. 2.

Genus _Artophormis_ Haeckel, 1882

Artophormis gracilis (Riedel, 1959)
(Plate **P4**, figure 6)

Artophormis gracilis n. sp. Riedel, 1959, p. 300, pl. 2, figs. 12, 13.
Artophormis gracilis Riedel; Moore, 1971, p. 742, pl. 5, figs. 10, 11; Sanfilippo et al., 1985, pp. 666, 667, figs. 12.2a, 12.2b, 12.2c; Nigrini et al., 2006, p. 26, pl. P3, figs. 20–22.
Cyrtophormis gracilis (Riedel); Petrushevskaya and Kozlova, 1972, p. 547, pl. 28, figs. 13–15.

Genus _Siphocampe_ Haeckel, 1882

Siphocampe nodosaria (Haeckel, 1887) group
(Plate **P3**, figures 8, 30)

Lithomitra (Lithomitrella) nodosaria n. sp. Haeckel, 1887, p. 1484, pl. 79, fig. 1.
Lithomitra nodosaria Haeckel group; Petrushevskaya, 1975, p. 586, pl. 10, fig. 18.

Siphocampe nodosaria (Haeckel); Nigrini and Lombari, 1984, N191, N120, pl. 32, fig. 3.

Remarks. This species differs from *Siphocampe arachnea* Haeckel group mainly by having less pores in each segment.

Siphocampe sp. B
(Plate **P3**, figures 26, 27)

Genus _Artostrobus_ Haeckel, 1887

Artostrobus cf. _semazen_ Renaudie and Lazarus, 2012
(Plate **P3**, figure 35)

Artostrobus semazen n. sp. Renaudie and Lazarus, 2012, p. 44, pl. 4, figs. 5A, 5B, 10, 13.

Remarks. The specimen shown in Plate **P3**, figure 5, is very similar to *Artostrobus semazen* Renaudie and Lazarus but differs by having a nearly cylindrical abdomen instead of fusiform. Considering it may be an intraspecific variation, we propose the name *Artostrobus* cf. *semazen* Renaudie and Lazarus.

Genus _Tricolocapsa_ Haeckel, 1887

Tricolocapsa sp. A
(Plate **P3**, figure 24)

Tricolocapsa sp. B
(Plate **P3**, figure 25)

Genus _Carpocanopsis_ Riedel and Sanfilippo, 1971

Carpocanopsis cingulata Riedel and Sanfilippo, 1971
(Plate **P4**, figures 7, 8)

Carpocanopsis cingulatum n. sp. Riedel and Sanfilippo, 1971, p. 1597, pl. 2g, figs. 17–21; pl. 8, fig. 8.

Carpocanopsis cingulata Riedel and Sanfilippo; Sanfilippo et al., 1973, p. 224, pl. 6, figs. 5, 6; Nigrini and Lombari, 1984, N87, N88, pl. 21, fig. 4.

Genus _Acrobotrys_ Haeckel, 1882

Acrobotrys disolenia (Haeckel, 1887)
(Plate **P3**, figure 29)

Acrobotrys disolenia n. sp. Haeckel, 1887, p. 1114, pl. 96, fig. 10.

Acrobotrys disolenia Haeckel; Kamikuri, 2019b, pl. 18, fig. 30.

Genus _Dendrospyris_ Haeckel, 1882

Dendrospyris aff. _bursa_ sensu Kamikuri, 2019a
(Plate **P4**, figures 19, 20)

Dendrospyris aff. *bursa* (Sanfilippo and Riedel); Kamikuri 2019a, pl. 7, figs. 12, 13.

Dendrospyris sp. A
(Plate **P4**, figure 21)

Dendrospyris sp. B
(Plate **P4**, figure 22)

Genus _Tholospyris_ Haeckel, 1882

Tholospyris mammillaris (Haeckel, 1887)
(Plate **P4**, figure 13)

Dictyospyris (Dictyospyrissa) mammillaris n. sp. Haeckel, 1887, p. 1076, pl. 89, figs. 9, 10.

Tholospyris mammillaris (Haeckel); Nigrini and Lombari, 1984, N73, N74, pl. 20, figs. 3a, 3b.

***Tholospyris* spp.**
(Plate **P4**, figures 14–18)

Genus *Trissocyclus* Haeckel, 1882

***Trissocyclus stauroporus* (Haeckel, 1887)**
(Plate **P4**, figure 9)

Zygostephanus (Zygostephus) dissocircus n. sp. Haeckel, 1887, p. 971, pl. 93, fig. 1.
Zygostephanium dizonium n. sp. Haeckel, 1887, p. 973, pl. 93, fig. 3.
Trissocyclus (Tricyclarium) stauroporus Haeckel, 1887, p. 987, pl. 83, fig. 5.
Liriospyris stauropora (Haeckel); Goll, 1968, pp. 1431, 1432, pl. 175, figs. 1–3, 7, text-fig. 9.
Trissocyclus stauropora Haeckel; Petrushevskaya and Kozlova, 1972, p. 533, pl. 39, figs. 29–31; Sanfilippo et al., 1985, pp. 664, 665, figs. 11.1a, 11.1b, 11.1c.

Genus *Dorcadospyris* Haeckel, 1882

***Dorcadospyris simplex* (Riedel, 1959)**
(Plate **P5**, figure 1)

Brachiospyris simplex n. sp. Riedel, 1959, pp. 293, 294, pl. 1, fig. 10.
Dorcadospyris simplex (Riedel); Riedel and Sanfilippo, 1970, p. 523, pl. 15, fig. 6; Nigrini and Lombari, 1984, N37, N38, pl. 18, fig. 3.

***Dorcadospyris ateuchus* Ehrenberg, 1874**
(Plate **P5**, figure 2)

Ceratospyris ateuchus n. sp. Ehrenberg, 1874, p. 218.
Dorcadospyris ateuchus (Ehrenberg); Sanfilippo et al. 1985, p. 663, figs. 10.4a, 10.4b.

***Dorcadospyris alata* (Riedel, 1959)**
(Plate **P5**, figure 5)

Brachiospyris alata n. sp. Riedel, 1959, pp. 293, 294, pl. 1, figs. 11, 12.
Dorcadospyris alata (Riedel); Riedel and Sanfilippo, 1970, p. 523, pl. 14, fig. 5; Sanfilippo et al., 1985, pp. 661, 662, fig. 10.7.

Genus *Lychnocanoma* Haeckel, 1887

***Lychnocanoma elongata* (Vinassa de Regny, 1900)**
(Plate **P5**, figures 3, 4, 6, 8)

Tetrahedrina elongata n. sp. Vinassa de Regny, 1900, p. 243, pl. 2, fig. 31.
Lychnocanoma elongata (Vinassa de Regny); Sanfilippo et al. 1973, p. 221, pl. 5, figs. 19, 20; Kamikuri et al., 2012, pl. 2, fig. 11.

***Lychnocanoma* sp. A**
(Plate **P5**, figures 7, 9)

Genus *Thamnospyris* Haeckel, 1882

***Thamnospyris schizopodia* (Haeckel, 1887)**

Gorgospyris (Thamnospyris) schizopodia Haeckel, 1887, p. 1071, pl. 87, fig. 4.
Thamnospyris schizopodia (Haeckel); Petrushevskaya and Kozlova, 1872, pl. 38, fig. 2.

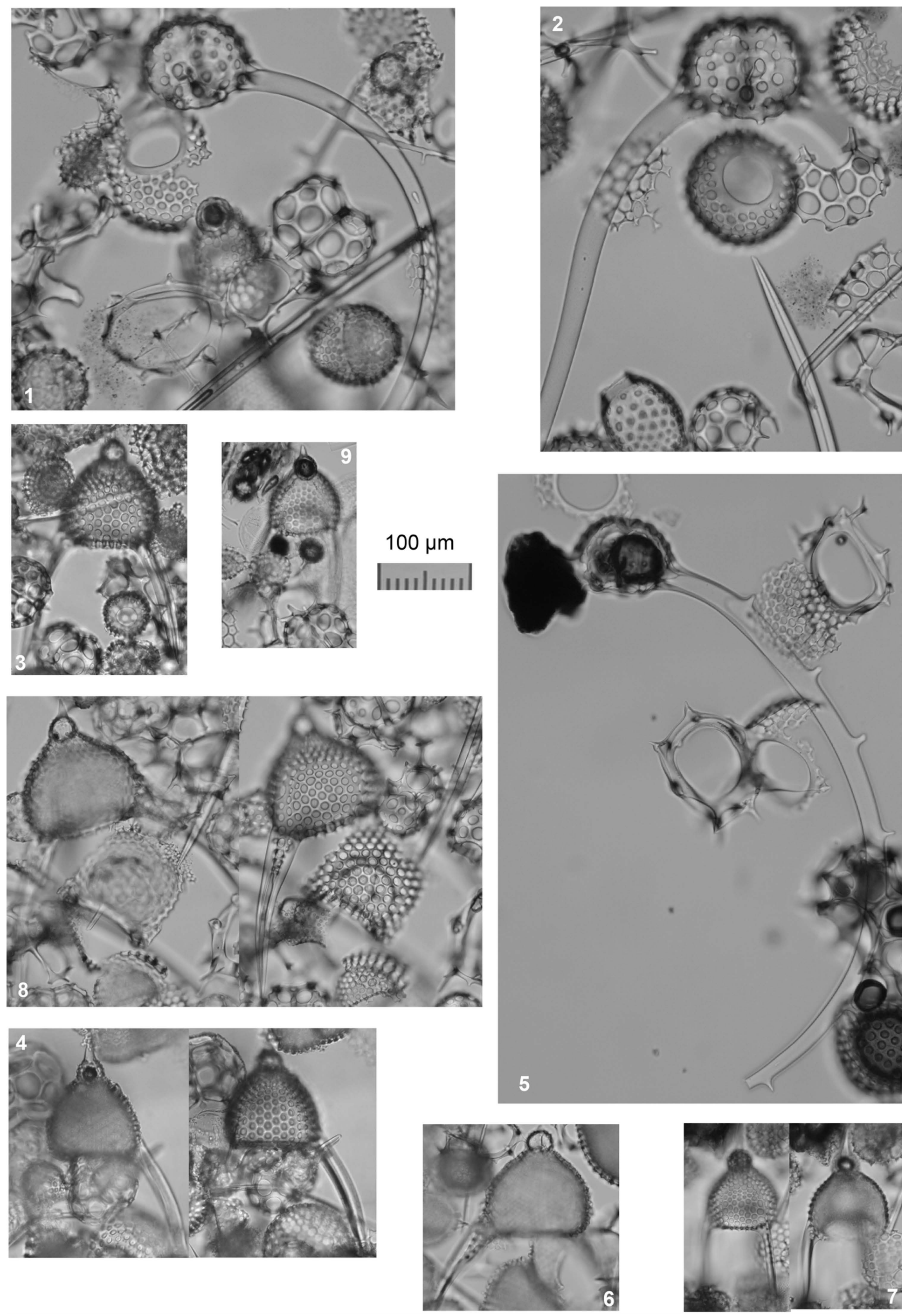

Plate P5. Radiolarians, Hole U1490A. 1. *Dorcadospyris simplex* (Riedel) (31F-CC). 2. *Dorcadospyris ateuchus* (Ehrenberg) (31F-CC). 3, 4, 6, 8. *Lychnocanoma elongata* (Vinassa de Regny) (3, 4: 41X-CC; 6, 8: 31F-CC). 5. *Dorcadospyris alata* (Riedel) (24H-CC). 7, 9. *Lychnocanoma* sp. A (35X-CC).